Image-, fluorescence- and radio-guided navigation for identification and localization of lymph node metastases in prostate cancer

Nienke Johanna Maria Klaassen

31 May 2018

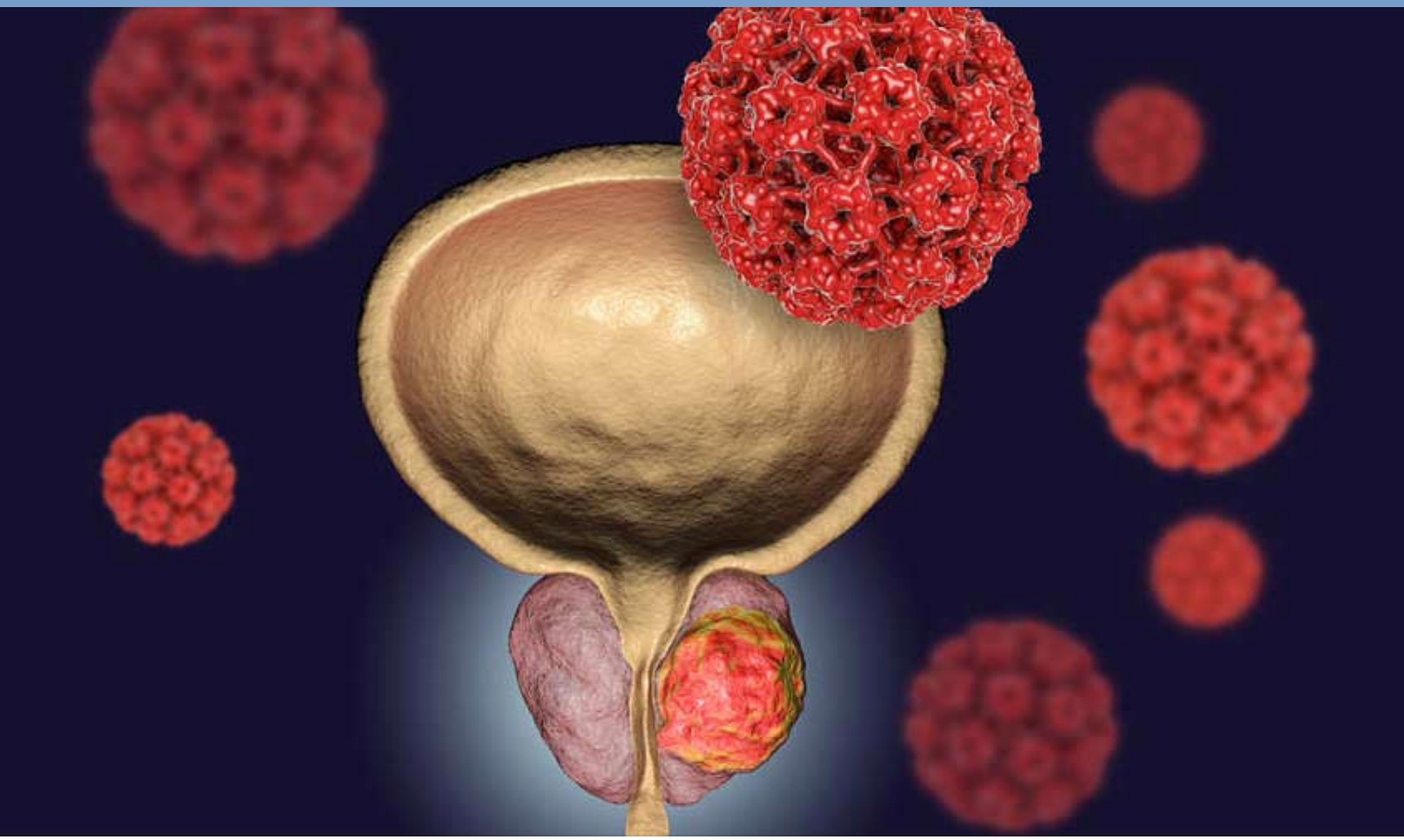

Radboudumc

UNIVERSITEIT TWENTE.

Image-, fluorescence- and radio-guided navigation for identification and localization of lymph node metastases in prostate cancer

Thesis

Graduation committee

Prof. dr. Ir. C.H. Slump – Chairman & Technical Supervisor

Prof. dr. J.J. Fütterer – Clinical Supervisor

Dr. M. Rijpkema – Technical Supervisor Radboudumc

Drs. P.A. van Katwijk – Process Supervisor

T.R.F. van Steenbergen MSc. – Daily Supervisor

Dr. A.T.M. Belos-Grob – External Member Graduation Committee

Table of content

Preface

Before you lies the master thesis 'Image-, fluorescence- and radio-guided navigation for identification and localization of lymph node metastases in prostate cancer'. The research for this thesis has been conducted in the Radboudumc. This thesis has been written in the context of my graduation assignment for the master Technical Medicine of the University of Twente and commissioned by the department of Radiology and Nuclear Medicine of the Radboudumc. I was engaged in researching and writing this thesis from June 2017 to May 2018.

My research question was formulated together with my supervisors Jurgen Fütterer, Mark Rijpkema and Thomas van Steenbergen. The research was challenging, but conducting extensive investigation has allowed me to answer the research question. Fortunately, my supervisors of the Radboudumc, Jurgen Fütterer, Mark Rijpkema and Thomas van Steenbergen, and my supervisors of the University of Twente, Kees Slump and Paul van Katwijk, were always willing to answer my questions.

I would like to thank my supervisors for the pleasant supervising and their support during my graduation assignment. In addition, I wish to thank all participants of the study, without their collaboration this thesis would never have led to a success.

I would like to express a special thanks to Antoi Meeuwis and Desirée Bos, for their great help. Furthermore, I wish to thank my colleagues of the Nuclear Medicine and Intervention Radiology for the pleasant cooperation and sociability. I often discussed with them my research in an effective way and we had a lot of fun. My family and friends also gave me good advices, moreover they supported me morally during the process.

I hope you enjoy your reading.

Nienke Klaassen

Nijmegen, May 14, 2018

List of abbreviations

800CW	IRDye 800CW
CT	Computed Tomography
ePLND	extended Pelvic Lymph Node Dissection
ICG	Indocyanine Green
SPECT	Single Photon Emission Computed Tomography
MRI	Magnetic Resonance Imaging
PBS	Phosphate Buffered Saline
PCa	Prostate cancer
PET	Positron Emission Tomography
PSA	Prostate Specific Antigen
PSMA	Prostate Specific Membrane Antigen
ROI	Region Of Interest
RP	Radical Prostatectomy
tPLND	targeted Pelvic Lymph Node Dissection

1. General introduction

Prostate cancer (PCa) is one of the most commonly diagnosed cancers in men, with approximately 1.1 million newly diagnosed men worldwide in 2012 [1]. With an estimated 307,000 deaths in 2012, PCa is the fifth leading cause of death from cancer in men [1]. Diagnosing PCa is based on determining the levels of prostate-specific antigen (PSA), Prostate imaging and prostate gland biopsy [2]. Magnetic Resonance Imaging (MRI) and Positron Emission Tomography (PET)/Computed Tomography (CT) are imaging modalities to localize the tumor area and detect possible metastases. MRI is the technique of choice to assess the tumor size, location and stage [3, 4]. MRI is highly sensitive to cancer due to recognizable regions and high contrast for soft tissue, whereas PET/CT, in addition to delimiting the global location of the tumor, might also detect potential distant metastases [5, 6].

A distinction can be made between four different stages of PCa. In the first two stages cancer lesions are limited to the prostate and therefore is called localized PCa. In the third stage, the tumor lesion has spread outside the prostate into nearby tissues, for example the seminal vesicles or urethras. In the fourth stage the cancer has spread to distant organs or lymph nodes. Besides the different stages of prostate cancer, a histopathological division can also be made based on the aggressiveness of the tumor tissue. The degree of aggressiveness is expressed by means of the Gleason scale. The Gleason scale scores the tissue obtained by biopsy based on differentiation, ranging from 1 to 5. Well differentiated tissue, also called low-grade PCa, is scored a 1 and poorly differentiated tissue, also called high-grade PCa, is scored a 5. The resulting Gleason score is determined by adding the two most dominant Gleason variants found in the tissue specimens.

The stage and Gleason score determine the possible treatment options. For men who suffer from primary PCa there is a wide array of treatment options. Patients with low-grade localized primary PCa are often kept under active surveillance, during which the tumor is monitored by determination of the PSA levels, repeating prostate biopsies and MR scans [2]. Treatment options for high-grade primary PCa are external beam radiation therapy, radical prostatectomy (RP) and brachytherapy [7, 8]. RP is considered as the gold standard to treat PCa [9, 10]. Although the survival rates of primary prostate cancer are relatively high, the odds become less favorable, when lymph node involvement is present [11].

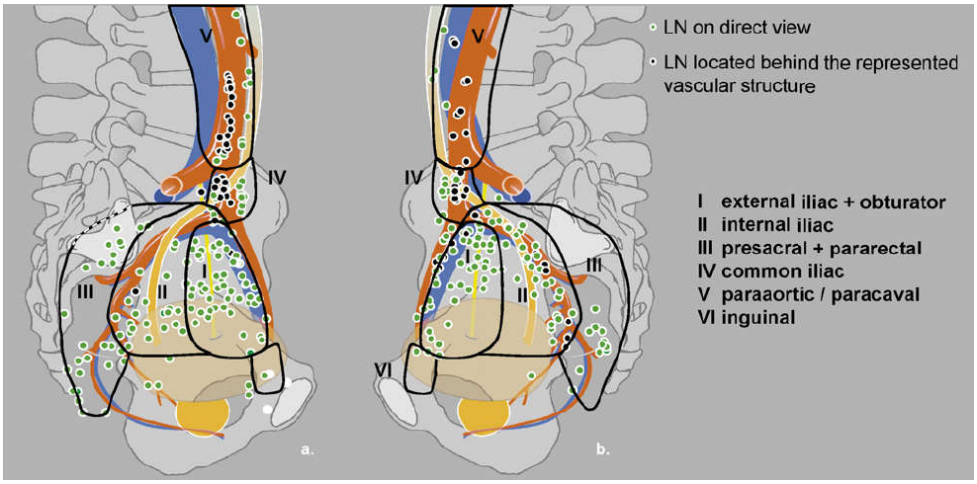

Figure 1: Primary lymphatic landing sites of the prostate in anterior-posterior projection of the pelvic, a) shows a reconstruction of the left hemipelvis and b) shows a reconstruction of the right hemipelvis. Most lymph node metastases are found in the external iliac (I) internal iliac (II) and obturator fossa (I) [16]

In approximately 25% of the patients with PCa, lymph node involvement is present. Most common sites for lymph node metastases are the obturator fossa (where in 60-89% of the cases lymph node involvement was seen) external iliac (36-83%) and internal iliac nodal areas (44-58%) (Figure 1) [12, 13]. The presence of lymph node involvement has been proven to be predictive for disease progression and biochemical recurrence rates [14]. Using the available imaging modalities, it might be challenging to detect whether lymph nodes are involved [10]. Therefore, lymph node metastases might be missed easily.

Extended pelvic lymphadenectomy (ePLND), in which the lymph nodes of the external iliac, obturator and interenal iliac areas are resected bilaterally, is considered as the gold standard to identify and treat lymph node involvement in patients with intermediate- and high- risk disease [10, 17, 18]. A study of Weingärtner et al. showed that on average 20 lymph nodes have to be resected to ensure an adequate and representative pathology sample [19]. During ePLND on average 21 to 28 [20, 21] lymph nodes are resected, therefore ePLND should ensure an adequate and representative sample. Despite the benefits of ePLND, this technique also has some shortcomings. First, a large number of pelvic lymph nodes are removed, causing a comprehensive disruption of the pelvic lymphatic anatomy. This disruption of the pelvic anatomy causes 75% of all complications after ePLND [22]. These large amounts of pelvic lymph nodes are removed regardless of whether lymph node infiltration is present or not. Therefore complications may also occur when lymph node infiltration is not present, which therefore represents overtreatment. Second, due to limited visualization and variations between patients, involved lymph nodes might still be missed resulting in undertreatment of these patients [10, 13, 16]. Especially lymph nodes localized in the para-aortic/paracaval and pararectal/presacral nodal regions are regularly missed [16]. Third, as already mentioned on average 21 to 28 lymph nodes are removed during ePLND.

Although these numbers ensure sufficient nodal removal in most cases, especially in high-grade PCa, involved lymph nodes might be missed, with distance metastases consequentially.

In order to prevent distant metastases and limit complications, all involved lymph nodes have to be resected and unaffected lymph nodes have to be left unthreatened. ePLND is unable to meet these requirements as a result of its disadvantages. Although pre-operative imaging using MRI, CT or PET is a good starting point, the pre-operative setting may differ from intra-operative setting. This shift between pre-operative and intra-operative setting is especially seen in soft tissue, with deviations of one to two centimeters observed in clinical practice. Therefore, there is need for intra-operative techniques to detect and visualize tumor deposits real-time. Studies have already been performed in which nanocolloid was injected into the prostate gland to search for sentinel nodes [23-25]. Although some advantages have been seen, this technique does not offer significant benefits compared to ePLND. In addition, studies have been performed using different ways of Prostate Specific Membrane Antigen (PSMA) targeting guidance [26, 27] and different techniques of image-guided navigation [28, 29]. Even though these techniques have their own advantages, a technique which; specifically targets PCa lesions, captures soft tissue shift, provides real-time feedback, and provides an approximated direction at distant and a substantially exact location close to a lesion, has not been found yet. Therefore during this study, which will be performed in the context of my graduation assignment in Technical Medicine, we will search for a specific, accurate and real-time navigation method to detect lymph node metastasis during surgery. The research question of this study is: "Which navigation technique adds value to identification and localization of lymph node metastases in patients with primary prostate cancer during pelvic lymph node dissection?"

First, a review focused on navigation techniques applicable to targeted pelvic lymph node dissection (tPLND) will be performed. The results of this literature review will form the basis for my study design.

2. Review

2.1. Methods

For the literature review databases PubMed, Scopus and Medline have been used. The aim of the literature review was to generate an overview of intra-operative navigation techniques applicable for tPLND. The first part of the literature study was limited to reviews of intra-operative navigation methods. This resulted in an overview of available navigation techniques, motivated on the basis of the suitability for our application. On basis of the first literature search we have generated a demarcated direction for intra-operative navigation for tPLND. The second part of the literature study was focused on the specific features of optical and electromagnetic navigation and radio- and fluorescence-guided navigation; image-guided navigation, ^{99m}Tc-nanocolloid, ^{99m}Tc-PSMA, IRDye 800CW-PSMA, and combined ^{99m}Tc-800CW-PSMA. The search terms used for the second part were: "prostate cancer", "hybrid intra-operative navigation", "^{99m}Tc-PSMA", "Fluorescent PSMA target", "IRDye 800CW-PSMA", "PSMA", "image-guided surgery", "infrared light tracking" and "electromagnetic field tracking".

2.2. Surgical navigation

In clinical practice, patients with intermediate- or high- risk prostate cancer are subjected to ePLND [17]. Although positive clinical results have been observed with this approach, metastatic lymph nodes are still being missed and in approximately 20% of the patients complications are being observed [16, 22].

Identification of metastatic lymph nodes during surgery can be improved using multiple methods. The first method comprises localization of sentinel lymph nodes. For this method ^{99m}Tc-nanocolloid is injected into the peripheral zone of both lobes of the prostate. After injection, the drainage pattern of the prostate to the lymph nodes is followed using Single Positron Emission Computed Tomography (SPECT)/CT . At 15 minutes (early stage) and 2 hours (late stage) post-injection, static SPECT/CT scans are made. Comparing these two scans facilitates localization of sentinel nodes pre-surgery. During surgery a gamma probe is used to localize the sentinel nodes intra-operatively via real-time acoustic feedback. Since the purpose of the sentinel node procedure is to visualize the drainage pattern of the prostate, it is unknown whether metastases are present in the found lymph nodes, prior to surgery. In addition, sentinel node procedures are not suited for identifying all lymph node metastatic drainage patterns, due to probable blockage of lymphatic drainage by cancer cells in patients with a serum PSA above 20 ng/mL and significant nodal involvement [25]. In a significant number (31%) of positive lymph nodes the cancer cells prevent the tracer from accumulating, whereby positive lymph nodes go undetected [25]. In case positive lymph nodes have been identified, sentinel lymph node mapping is followed by ePLND, in which 21-28 lymph nodes in predefined regions are being removed [20, 21]. A systematic review of 20 studies indicates that, when the results of the lymph node mapping would not be taken into account during ePLND, metastatic lymph nodes in one in the 20 patients would be left behind [30].

Another method is based on specific targeting of tumor lesions instead of sentinel lymph nodes. The Prostate Specific Membrane Antigen (PSMA) is a transmembrane protein which is overexpressed on prostate tumors and metastases originating from prostate tumors. In around 90% of all prostate tumors and metastases expression of PSMA can be observed [31]. Due to the overexpression of PSMA on PCa lesions, radiotracers labeled with PSMA can be used for specific localization of PCa and metastases [32, 33]. ^{68}Ga-PSMA is a ligand which is used in clinical practice to image PCa using a PET/CT scanner. Radiotracers labeled with PSMA might also be used to guide the surgeon to lymph node metastases during Pelvic Lymph Node Dissection (PLND). For this application labeled PSMA ligands are intravenously administrated to the patient prior to surgery, to which it find its way to the PCa lesions. During surgery a gamma probe is used to localize the targeted PCa lesions, just like the sentinel node procedure. Studies have been performed in which PSMA was labeled with ^{99m}Tc [26, 28, 34] and ^{111}In [35] for surgical navigation. ^{99m}Tc-PSMA seems to have more potential compared to ^{111}In-PSMA, as a result of lower costs and wider availability of the radiotracer [26].

Since targeted radio-guidance is based on real-time acoustic feedback, delineation of the tumor lesions remains inaccurate. Although radio-guidance is a good tool for detection, visual feedback is needed to obtain a higher accuracy. Therefore for a more accurate navigation method, the radiotracer might for example be combined with a fluorescent marker as well. An example of a frequently used fluorescent marker is indocyanine green (ICG). ICG is already used in combination with ^{99m}Tc nanocolloid to visualize sentinel lymph nodes, which has potential but still faces the limitations of sentinel node mapping as mentioned earlier [36, 37]. Brouwer et al. performed a phantom study and clinical trial in which they combined ICG fluorescence-guidance during surgery and a SPECT/CT ^{99m}Tc-PSMA scan, the results of this study show the feasibility of this combined approach [28]. The disadvantage of ICG is that this fluorescent marker cannot be covalently coupled to a tumor-targeting tracer, since it has no reactive chemical group for labeling to for example a PSMA ligand [38]. The use of monoclonal antibodies to target PCa has shown limited success as a result of low permeability in solid lesions and a long circulating plasma half-life [39]. Another fluorescent marker is IRDye 800CW (800CW). Matsuoka et al. developed a small molecule succinimidyl-Cys-C(O)-Glu (SCE) which they labeled with 800CW [40, 41]. 800CW-SCE showed a high selective binding affinity to PSMA in vitro but it has to be optimized to become an useful ligand for PSMA targeting [40].

PSMA labeled radiotracers and fluorescent markers are useful for identification and localization of metastatic lymph nodes. Though, in some regions it is hard to find the exact location of lymph nodes, regardless of whether PSMA labeled radiotracers are used or not. This limitation is especially seen in the para-aortic/paracaval and pararectal/presacral nodal regions. Both ICG and 800CW are near-infrared fluorescent dyes and have a penetration depth of maximally 10mm [42, 43]. However, in clinical practice the penetration depth is only 2-3 mm, as a result of which only nearby lesions can be found. In addition, studies emphasize the challenging character of navigating to the exact tumor location based on detection of

^{99m}Tc alone, for example as result of the background activity at the injection side during sentinel node procedures [44]. To overcome the shortcomings of 800CW and ^{99m}Tc detection during surgery, the use of pre-operative images might be helpful to navigate close enough towards involved lymph nodes. Research has been performed regarding intra-operative navigation using pre-operative images. This type of navigation is called image-guided navigation. The vast majority of image-guided navigation options are aimed at navigation within bony structures [45, 46], but navigation techniques for soft tissue have been studied as well [46-48].

One of the most important aspects in image-guided surgery is the linkage of the pre-acquired images with the settings in a patient during surgery. High resolution CT and MRI are imaging modalities which are most frequently used for the image acquisition, but other imaging modalities may be used as well. The linkage of images with the intra-operative setting is called registration. Registration can be performed either by point merge systems, that match preselected points using tracking techniques, or by surface topography [42]. Point merge systems use anatomical landmarks within the body or fiducial landmarks which are attached to structures to perform registration. Point merging is rigid and does not take deformation into account. Therefore, most research using point merge systems has been performed in non-deformable structures, such as bones [49-51]. However, research is not only limited to non-deformable tissue. Navigation in deformable structures, such as liver and prostate, has also been studied [48, 52]. Results show difficulties for registration in deformable structures using point merge systems as a result of shift of the tissue, but potential has been seen in surface topography matching [46, 53]. Surface topography matching can be performed in various ways, e.g., using ultrasound or laser. Brainlab, one of the commercial navigation systems, has developed a tool, Z-touch, in which the principle of surface topography using a laser is used for registration. Although surface matching registration systems using laser are promising, they are not as accurate as point merge systems. In studies of surface scanning using the Z-touch, a larger amount of registration errors have been observed compared to registration based on fiducial landmarks [54, 55]. Surface matching using ultrasound has some advantages e.g., real-time, accurate and detailed information, but also faces some limitation as a result of large variability in image quality due to differences between users and settings of the ultrasound probe [42]. A combination of point merge and surface topography matching is point cloud registration. For point cloud registration points are touched and marked with a pointer and correlated with the surface of segmented pre-performed imaging. When the points are selected on rigid tissue the match is relatively good, but in soft tissue this might cause deviation.

Tracking of surgical instruments depends on the type of navigation system used. Image-guided navigation systems can be based on a variety of techniques e.g., electromagnetic fields, sound waves, infrared light, and other techniques. The most frequently used navigation systems use electromagnetic field or infrared light tracking. For electromagnetic field tracking sensors are used to determine the position of the patient and surgical instruments, whereas for infrared light tracking reflecting spheres are used for the position determination. The

position of the patient reference target relative to the instrument reference target is calculated in the navigation software. To determine the position of the instrument tip in relation to the reference target, instrument calibration has to be performed. (More details about the calculations of the positions using transformation matrices can be found in appendix II.)

The two most applied image-guidance techniques i.e., electromagnetic field and infrared light tracking, have their own advantages. The most prominent advantage of electromagnetic field tracking is that the line-of-sight does not need to be maintained during tracking, whereas for infrared light tracking the line-of-sight can be disturbed as a consequence of positioning [56]. The maintenance of the line-of-sight between the camera and the patient and instrument is of importance in infrared light tracking, since disturbance of this line-of-sight results in the loss of navigation. A disadvantage of electromagnetic field tracking is the limited work field of 42x60x60 cm of the Aurora V2 Tabletop Field Generator and 50x50x50 cm of the Aurora V2 Planar Field Generator (Northern Digital Inc, Waterloo, Canada) [57, 58]. Brainlab uses the Aurora V2 Planar Field Generator for their electromagnetic tracking. The work fields of the field generators become even smaller by the use of metal surgical instruments.

For the visualization of the anatomical location different techniques can be applied as well, the anatomical location may be displayed on a screen, augmented reality glasses or projected in the surgeon's field of view[59-61].

The navigation techniques discussed in this review have their own advantages and disadvantages. A navigation technique that supports the surgeon during PLND should; perform specific targeting, capture soft tissue shift, provide real-time feedback and be accurate.

Specific targeting can be obtained using PSMA ligands. Although radio labeled ligands allow detection of metastatic lymph nodes at a distance, delineation of tumor lesions is almost impossible. The opposite is seen by fluorescent labeled ligands, delineation of the tumor at a distance of a couple of millimeters can be performed, however after these couple of millimeters fluorescent detection becomes inaccurate. Combining both techniques might overcome their disadvantages.

Real-time visual feedback can be obtained by image-guided navigation, as a result of pre- and intra- operative imaging. However, image-guided navigation alone does not provide millimeter accuracy in deformable tissue [29, 62]. Since PSMA ligands bind specifically to PSMA, which is overexpressed on prostate tumor cells, this type of navigation is independent from tissue shift. A combination of image-guided and PSMA ligand guided navigation might eliminate the disadvantage of soft tissue navigation.

Therefore, our hypothesis is that a combination of image-guided navigation and intra-operative radio- and/or fluorescence-detection will result in a more accurate tPLND.

To test our hypothesis, in **Chapter 3** we will study the possibility of distinguishing affected and unaffected lymph nodes using radio- and image-guided navigation in a phantom study. Since metastatic lymph nodes might be located near draining organs, the delectability of lymph nodes with and without organ background will be compared as well. The purpose of **Chapter 4** is to study the penetration depth of a fluorescent dye (IRDye 800CW), in order to test the applicability of fluorescence for PLND. This penetration depth will be studied based on dye concentrations which may occur in patients, and in three types of tissue i.e.; muscle, fat and connective tissue. **Chapter 5** provides a brief overview of a clinical pilot study regarding radio-guided tPLND which will be designed. In **Chapter 6** a general discussion on this thesis can be found. In the end of this chapter some future perspectives are considered.

3. Phantom study hybrid navigation

3.1. Abstract

Introduction: Prostate cancer is one of the most frequently seen types of cancer in men. The survival rates are relatively high, but decrease significantly when metastases are present. Nowadays, extended pelvic lymph node dissection is performed to remove potential metastatic lymph nodes. Although, extended pelvic lymph node dissection is associated with positive outcomes, negative results and high complication rates have been seen as well. Therefore, targeted pelvic lymph node dissection might be beneficial. Targeting could be performed in various ways e.g., using fluorescence-, radio-or image-guidance. In this study we focused on the application of radioactivity and image-guidance.

Methods: A phantom, composed of the lids of a NEMA and Micro Hollow Sphere Phantom and the cylinder of a Jaszczak Phantom, was used to study the distinguishability of affected from unaffected lymph nodes. Real patient data was used as input for the phantom study. Activity calculations of lymph nodes, bladder, kidneys and lesions within the prostate were performed using 27 [^{68}Ga]Ga-PSMA-HBED-CC PET/CT scans, these activities were used in the phantom. Seven readers were questioned to identify spheres containing radioactive solution in the phantom, via acoustic gamma detection and image-guided navigation. The first experiment was aimed at acoustic gamma detection without background activity, the second experiment was aimed at acoustic gamma detection with background activity, and the third experiment was aimed at hybrid guidance with background activity.

Results: The results of our study show that positive lymph nodes are significantly better distinguishable from negative lymph nodes when the probe can be placed closer to the lymph nodes. We also observed a significant influence of background organ activity on the distinguishablity of positive and negative lymph nodes. At a distance of 0 cm to the lymph nodes a significant larger percentage of spheres was identified correctly when no background activity was present compared to the situation in which background activity was present. In case only image-guided navigation was applied, approximately half of the readers identified the active sphere incorrectly. Using hybrid navigation we observed an significant increase in correct identification.

Conclusion: Both radio- and image-guidance are feasible techniques to distinguish affected form unaffected lymph nodes in the pelvic region during surgery. However, hybrid navigation seems to be feasible and superior compared to any guidance technique alone.

3.2. Introduction

Prostate cancer (PCa) is, with an incidence of approximately 85 per 100.000 in western Europe in 2012, one of the most prevalent forms of cancer in men [1]. Although the survival rates are, with a 5-year survival rate of 90%, relatively high in case of localized prostate cancer, these numbers decrease significantly by the presence of metastases (5-year survival rate of 29%)[11]. To prevent spread of the disease, it is important to detect and remove all probable metastatic lymph nodes. Nowadays, it is attempted to remove all pelvic lymph nodes, regardless of whether metastases are present or not, via extended pelvic lymph node dissection (ePLND) [10]. However, visualization within the pelvic region is limited and anatomy between patients varies, which might cause lymph nodes to be missed [10, 13, 16]. In addition to metastatic lymph nodes being missed, a large amount of healthy lymph nodes are removed causing 75% of all complications after PLND [22]. Specific identification of prostate cancer lesions might be helpful for targeted removal .

In clinical practice a ^{68}Ga-PSMA PET/CT scan is performed in patients suspicious for prostate cancer. The ^{68}Ga-PSMA tracer specifically binds to the Prostate Specific Membrane Antigen (PSMA) which is overexpressed on tumor lesions originated from prostate cancer [32]. Due to the specific binding of the PSMA ligand, lymph node metastases could be detected as well [32]. Besides pre-operative detection and imaging of tumors, targeted radiolabeling might also make detection of metastatic lymph nodes easier during surgery. ^{68}Ga-PSMA is a well-accepted tracer for imaging prostate cancer, though since the half-life of ^{68}Ga is approximately one hour, this radionuclide is unfavorable for lymph node detection during surgery. ^{111}In-PSMA and ^{99m}Tc-PSMA are tracers suitable for lymph node detection during surgery, since both ^{111}In and ^{99m}Tc are detectable by a gamma probe. The half-lives of the two radionuclides differ, ^{111}In has a half-life of approximately 2.8 days and ^{99m}Tc a half-life of approximately 6 hours. In addition to the favorable half-life, ^{99m}Tc is also a pure gamma emitter in contrast to ^{111}In, making ^{99m}Tc more attractive to use during surgery compared to ^{111}In.

Metastatic lymph nodes might still be missed using radioactive navigation alone, due to the position of lymph nodes near active organs or in regions where visualization is impaired. Image-guided navigation, in which navigation is performed intra-operatively using pre-operative images, could provide a solution, since the pre-operative images are used as a map during surgery to navigate to a specific location. Therefore, hybrid navigation, in which radioactive and image-guided navigation are combined, might be an improvement.

The aim of this study was to detect whether it is possible to distinguish affected from unaffected lymph nodes in the pelvic region using ^{99m}Tc and image-guided navigation in a phantom model. Since lymph nodes might be located next to active organs, the detectability of lymph nodes with and without organ background was compared.

3.3. Methods and Materials

To study the impact of distance, isotope activity, and organ background activity on the detectability of active lymph nodes, the study was divided in an activity calculation part and three phantom studies.

Figure 2: Image of a [^{68}Ga]Ga-PSMA-HBED-CC PET-CT scan with ROIs drawn around the kidneys (blue arrows) and an positive lymph node (red arrow)

3.3.1. Activity Determination

27 [^{68}Ga]Ga-PSMA-HBED-CC ([^{68}Ga]PSMA) PET/CT scans, performed between 01-08-2017 and 31-08-2017, were selected to quantify the mean activity in the kidney, bladder and cancer lesions in the prostate. All scans were performed with the Biograph 40 mCT scanner (Siemens Healthineers, Erlangen, Germany), which combines a three-dimensional time of flight (TOF) PET scanner and a CT scanner. A CT scan was used for attenuation correction. The PET data was reconstructed using the UltraHD-PET (TrueX + TOF) reconstruction algorithm. The images were reconstructed in 256x256 matrices with a voxel size of 2x2x2 mm. For all reconstructions, 3 iterations and 21 subsets were applied and a Gaussian filter with 7.5 mm FWHM was used.

20 of the 27 [^{68}Ga]PSMA scans contained suspicious lymph nodes. 12 of the 20 scans containing suspicious lymph nodes were selected based on physicians' report to quantify the highest, mean and smallest activity in a total of 24 suspicious lymph nodes. Quantification was performed using Inveon Research Software of Siemens Healthineers. For the mean organ activity in 4 of the 12 scans the kidneys were quantified and in 5 of the 12 scans the bladder

was quantified. In addition, 7 lesions in the prostate out of 4 scans were quantified. Regions of Interest (ROI's) were drawn with a small margin around the tumor lesions, lymph nodes and organs. All ROI's were drawn in coronal view, and checked in axial and sagital view. Inside each ROI the maximum voxel value was determined and used for thresholding. A threshold of 50% of the maximum voxel value was applied to each ROI. As a result, ROI's were created containing voxels with only a higher value than the threshold value. An example of the drawn ROI's can be seen in Figure 2. Using the drawn ROI's the lowest activity measured in the lymph nodes, the mean activity of the lowest eight lymph nodes, the mean activity of the middle eight lymph nodes, and the mean activity of the highest eight lymph nodes were determined (Table 1). In addition, the mean activities in the kidneys, bladder and lesions in the prostate were determined (Table 2).

Table 1: Measured lymph node activities in 24 suspicious lymph nodes

Measured lymph node activities (Bq/mL)	
Smallest activity measured	852.6
Mean of eight smallest activities	3009.2
Mean of eight middle activities	4581.5
Mean of eight highest activities	13075.7

Table 2: Mean activity in organs. Kidney activity measured in four patients, bladder activity was measured in five patients and seven prostate lesions were determined in four patient

Measured activity in organs (Bq/mL)	
Mean activity Kidneys	38863.1
Mean activity Bladder	9717.3
Mean activity lesions in Prostate	4551.6

3.3.2. Phantom Studies

For the phantom studies a phantom was designed which was composed of the lids of two phantoms with spheres of different sizes (Figure 3). The two phantoms used were a National Electrical Manufacturers Association (NEMA) International Electrotechnical Commission (IEC) Body Phantom Set, model PET/IEC-BODY/P (NEMA phantom) and a Micro Hollow Sphere Phantom, model ECT/HS/MMP (microphantom). The lid of the NEMA phantom has a diameter of 19 cm, containing six fillable spheres with an inner diameter of respectively 10, 13, 17, 22, 28 and 37 mm. The spheres were numbered according to their size, with 1 for the sphere with an inner diameter of 10 mm and 6 for the sphere with an inner diameter of 37 mm. The lid of the microphantom has a diameter of 33.5 mm, containing five fillable spheres with an inner diameter of respectively 4, 5, 6, 8 and 10 mm. Sphere numbering was continued, with 7 for the sphere with an inner diameter of 4 mm and 11 for the sphere with an inner diameter of 5 mm. The two lids were placed in the cylinder of a Jaszczak phantom with an inner diameter of 21.6 cm and a height of 18.6 cm and connected to the box with PMMA screws. The spheres with numbers 1 -3 and 7 – 11 mimic the lymph nodes and the largest spheres with number 4 – 6 mimic the organs.

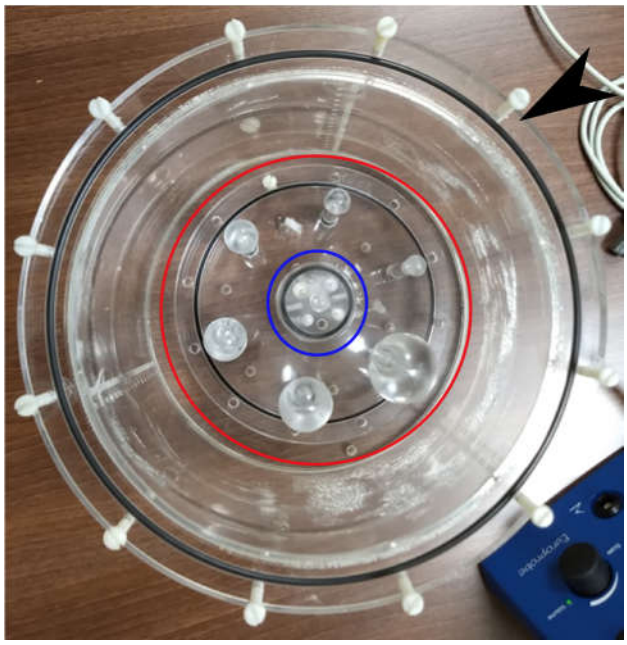

Figure 3: Image of the used phantom. Composed of the lid of the NEMA phantom (red circle) and the lid of the microphantom (blue circle) placed together in the cylinder of the Jaszczak phantom (black arrow).

Radioactive navigation

Both phantom studies aimed at radioactive navigation were performed in duplicate (Table 3). For the first phantom study four (experiment 1.1) and five (1.2) of the lymph node spheres were filled with 900, 3000, 4600 and 13100 Bq/mL ^{99m}Tc. For the second phantom study five (2.1) and four (2.2) of the lymph node spheres were filled with 900, 3000, 4600 and 13100 Bq/mL ^{99m}Tc. For the second phantom study the organ spheres were filled with 9700, 4600 and 38900 Bq/mL ^{99m}Tc. The injected activities in the spheres are summarized in Table 3.

Table 3: Injected activities per sphere. Spheres 4-6 are considered as organ spheres and have an approximated constant activity (experiments 2.1, 2.2 and 3.1) or no activity (experiments 1.1 and 1.2)

Experiments	Activity spheres (Bq/mL)										
	1	**2**	**3**	**4**	**5**	**6**	**7**	**8**	**9**	**10**	**11**
1.1	3000	-	-	-	-	-	-	-	4600	13100	900
1.2	-	900	3000	-	-	-	-	13100	900	4600	-
2.1	4600	-	900	9700	4600	38900	4600	3000	-	13100	-
2.2	-	4600	-	9700	4600	38900	3000	-	13100	-	900
3.1	-	-	-	9700	4600	38900	-	-	-	3000	-

Hybrid navigation

The phantom study aimed at hybrid navigation was performed in monoplo (3.1). For this phantom study one lymph node sphere was filled with 3000 Bq/mL ^{99m}Tc, and the organ spheres were filled with 9700, 4600 and 38900 Bq/mL ^{99m}Tc. Prior to the phantom study, the phantom was filled with ^{68}Ga in the same activities as used for the study. A PET/CT scan of the phantom was made with the Biograph 40 mCT scanner (Siemens Healthineers, Erlangen, Germany). This PET/CT scan was used as a map for the optical navigation system (Brainlab, Munich, Germany). The active spheres were drawn on the map, where the size of the lymph node spheres of the microphantom (7-11) were made equal to avoid bias. During the phantom study the lid of the microphantom was rotated 9 mm compared to the orientation in the scan, to mimic the deviation of soft tissue in clinical practice.

3.3.3. Data Acquisition

For the phantom studies aimed at radioactive navigation, seven readers were included. The readers were asked to indicate whether the spheres were filled with activity or not. The identification was performed via acoustic gamma detection (EuroProbe 3, EuroMedical Instruments, Paris France). In both phantom studies the organ spheres (4 – 6) were left out of consideration. The readers were asked to identify whether there was activity in each individual sphere (yes / no) at a height of respectively 10, 5 and 0 cm above the spheres, and whether they were reasonably sure or uncertain about their decision.

For the phantom study aimed at hybrid navigation, the same seven readers were approached to indicate the active spheres. The identification was performed using an optical navigation system (Brainlab, Munich, Germany) and the same acoustic gamma probe as used for the first series of experiments. The phantom study was divided in three parts. In the first part, the readers were requested to identify the active organ spheres, displayed on the optical navigation system, using an unconnected tracked gamma probe. This first part was intended as a training session. In the second part, the readers were asked to identify the active sphere in the middle part of the phantom (microphantom), using an unconnected tracked gamma probe. For the last part of the phantom study the gamma probe was connected to the acoustic gamma counter. The readers were asked to identify the active sphere in the middle part of the phantom again, but now using the optical navigation in combination with the acoustic gamma counter. For all these three parts the readers had to denominate the spheres containing radioactive solution on an answer form.

3.3.4. Data Analysis

All values were expressed as percentages of correctly identified spheres and the results were analyzed using ANOVA followed by post-hoc test. A p value of less than 0.05 was considered as statistically significant.

3.4. Results

A significant larger percentage of spheres was identified correctly in the experiments without background activity compared to the experiments with background activity at a distance of 0 cm to the spheres (83.93% ± 10.32 vs 68.75% ± 14.50; p=0.01) (Figure 4). When looking at the reasonably sure identifications, a significant larger percentage of spheres identified as reasonably sure activity can be observed in the experiments without background activity compared to the experiments with background at a distance of 5 (33.93% ± 13.36 vs 16.07% ±16.58; p=0.01) and 0 cm (76.79% ±13.74 vs 47.32% ±12.19; p=0.001). In case of the uncertain identifications, a significant lower percentage of uncertain identified spheres can be observed at all three distances; at 10 cm (25.00% ±19.61 vs 43.75% ±16.08; p=0.05), at 5 cm (20.54% ±11.61 vs 39.29% ±15.39; p=0.05), and at 0 cm (7.14% ±9.45 vs 21.43% ±17.29; p=0.01).

In the experiments without background activity, a significant larger percentage of correctly identified spheres can be seen at a distance of 0 compared to 10 cm (83.93% ± 10.32 vs 48.21% ± 17.58; p=0.001) and at 0 compared to 5 cm (83.93% ± 10.32 vs 54.46% ± 15.20; p=0.001). When looking specifically at the identifications which were identified as reasonably sure, significant larger percentages of spheres identified as reasonably sure can be found at 0 compared to 10 cm (76.79% ± 13.74 vs 23.21 ±20.13; p=0.001) and at 0 compared to 5 cm (76.79% ± 13.74 vs 33.93% ±13.36; p=0.001). A significant lower percentage of uncertain identified spheres can be observed at a distance of 0 compared to 10 cm (7.14% ±9.44 vs 25.00% ±19.61; p=0.01).

For the experiments with background activity, significant larger percentages of spheres have been identified correctly at 0 compared to 10 cm (68.75% ± 14.50 vs 53.57% ±7.64; p=0.01) and at 0 compared to 5 cm (68.75% ± 14.50 vs 55.36% ± 9.45; p=0.01). Looking at the sphere identifications where the participants were reasonably sure about their identification, a significant larger percentage of spheres identified as reasonably sure can be observed at a distance of 0 compared to 10 cm (47.32% ± 12.19 vs 9.82% ± 17.80; p=0.001) and at 0 compared to 5 cm (47.32% ± 12.19 vs 16.07% ± 16.58; p=0.001). A significant lower percentage of uncertain identified spheres can be observed at a distance of 0 compared to 10 cm (21.43% ±17.29 vs 43.75% ±16.08; p=0.01) and at 0 compared to 5 cm (21.43% ±17.29 vs 39.29% ±15.39; p=0.05).

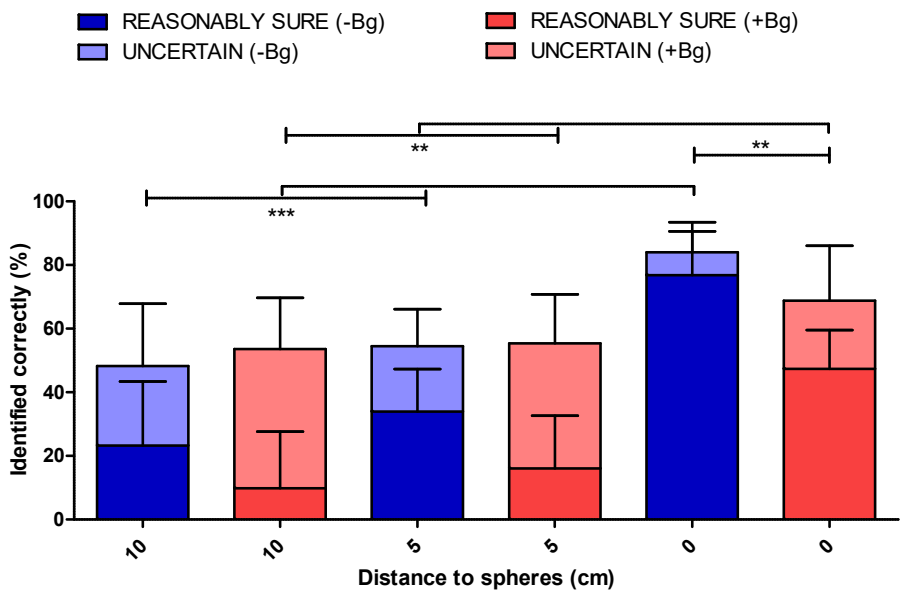

Figure 4: Percentages of correctly identified spheres (both positive and negative) for the experiments with (+Bg) and without background activity (-Bg) at three distances (10, 5 and 0 cm). Each bar is divided in; reasonably sure about their identification, and uncertain about their identification. Significant differences can be observed between the two groups for the total correctly identified spheres at a distance of 0 cm (p=0.01), for the total correctly identified spheres in the experiments without background at a distance of 0 cm compared to 5 and 10 cm (p=0.001), and for the total correctly identified spheres in the experiments with background at a distance of 0 cm compared to 5 and 10 cm (p=0.01).

In the phantom experiment in which only image-guidance was used, 3 readers indentified the active sphere correctly against 4 readers who identified the active sphere incorrectly (Figure 5). When looking at the combined image- and radio-guidance a significant larger percentage of the readers identified the active sphere correctly (100% correct vs 0% incorrect; p=0.001). A significant larger percentage of the readers identified the active sphere correctly using hybrid guidance compared to image-guidance (100% ±0 vs 42.86% ±53.42; p=0.05).

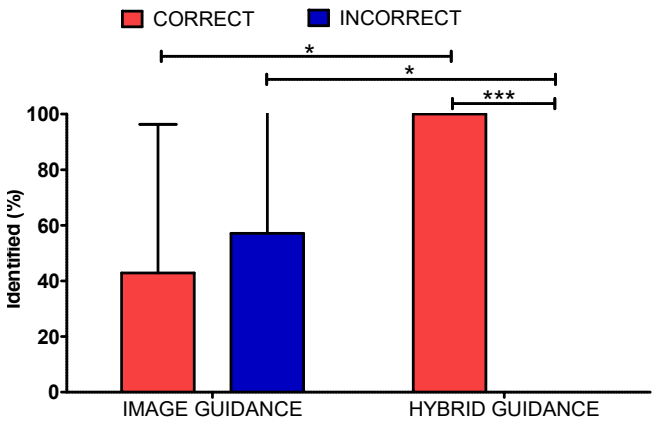

Figure 5: Percentages of correct and incorrect identification of the positive sphere using image - and hybrid-guidance, with a shift of 9 mm in the phantom compared to the prior performed scan. Significant differences can be observed for both the correct en incorrect identification between the two different approaches. Significant differences can be observed as well within the hybrid guidance.

3.5. Discussion

To mimic the situation of a patient with lymph node metastases, we composed a phantom study in which we used different navigation techniques. First we used radio-guidance. The results of this study showed that the detection accuracy improved when the probe can be placed closer to positive lesions. We also observed a significant influence of background activity of bladder, kidneys and prostate lesions on the distinguishablity of positive lymph nodes. Subsequently using image-guidance, the exact location can be reached approximately. However, the decision improved when both image- and radio-guidance were applied.

In sentinel lymph node procedures using ^{99m}Tc-nanocolloid the influence of background activity on the detectability of sentinel lymph nodes have been observed, especially near the injection site [44]. In our study we also observed a significant influence of background activity on detectability of metastatic lymph nodes. Since the targeted approach ensures more background activity compared to sentinel node procedures as a result of the intravenous administration of a labeled traces, the influence of the background activity will be more pronounced in the targeted approach compared to the sentinel node procedure. However, it is possible to tune the amount of background activity to some extent by studying the most favorable time between surgery and injection. Schaal et al. performed a clinical trial in which they injected ^{111}In-PSMA ligand 48 hours prior to surgery to allow clearance from the unbound ligand [35]. In a study of Vallabhajosula et al. the tumor to background ratio of a high-affinity small-molecule PSMA ligand which was labeled with ^{99m}Tc (^{99m}Tc-MIP-1404) was studied. This study showed a ratio of 3:1 at 1 hour post-injection and of 9:1 20 hours post-injection [65].

In our study we used ^{68}Ga-PSMA scans for activity determination. However, ^{99m}Tc-PSMA can, besides detection of lymph nodes during surgery, also be used to image prostate cancer lesions using SPECT/CT. However, the specificity of a ^{99m}Tc-PSMA SPECT/CT is worse compared to the specificity of a ^{68}Ga-PSMA PET/CT. Maurer et al. showed that in a study with 31 patients 44 lesions were observed with a ^{68}Ga-PSMA PET/CT scan versus 25 of these lesion with a 99mTc-PSMA SPECT/CT scan [63]. Therefore, since the distribution of ^{68}Ga-PSMA and ^{99m}Tc-PSMA is comparable [26, 34, 64], ^{68}Ga-PSMA PET/CT scans might be used as a map for the distribution of ^{99m}Tc-PSMA during surgery.

Since the disadvantage of the background activity can never be eliminated completely, a combination with image-guided navigation might be helpful. To mimic an intra-operative in human situation, in which organs and lymph nodes deviate as a result of soft tissue, we applied a deviation of 9 mm within our phantom. The shift of 9 mm ensured a situation in which the spheres of the microphantom in real life were positioned exactly in the between the spheres in the scanned situation. Our results showed that in case a deviation of 9 mm was applied within our phantom, almost 50% of our readers identified the positive sphere incorrectly. We chose to manipulate the phantom in this way to mimic non rigidity of tissue in combination with the influence of two structures located close to each other. Our results

suggests that, in one-time registration, a deviation of 9 mm has a noticeable influence on detectability of the right lymph node. However, we have to take into account that doubt arose between two spheres as a result of positioning of the sphere containing radioactive solution exactly in between two spheres in the pre-operative situation. Although it may also occur in a patient that it is unclear which of two adjacent lymph nodes is positive, this phenomenon does not always have to occur.

Baumhauer et al. also refer the non-rigidity of soft tissue as a limitation in one-time registration image-guided surgery, since the validity of the information presented can hardly be verified [62]. To overcome this limitation, it is important to identify the tissue shift. A way in which this could be performed is for example with laparoscopic ultrasound in case the tissue shift is caused by respiration. This approach is used, among others, in navigated liver resection and laparoscopic radiofrequency ablation [66]. Although, since this approach is aimed at tissue shift caused by respiration, this is not applicable for tissue shift in the pelvic region. Feuerstein et al. used surface adhesive markers which can detect the magnitude of tissue shift, allowing verification of navigation validity [67]. A similar approach has been applied in another study in which markers were placed in organs using a laparoscope. The markers register the shift from the inside, resulting in a reverse registration [68]. These studies show the difficulty of accurate navigation in soft tissue using image-guidance alone. Therefore, we indicate that hybrid navigation would add value to localization and identification of lymph nodes in the pelvic region.

Our results underline the added value of the use of hybrid navigation to localize metastatic lymph nodes. Studies have been performed in which hybrid navigation was used in PCa surgery [44, 69]. However, most of these studies were performed using nanocolloid. Therefore, further research has to be performed regarding hybrid navigation based on a targeted approach.

The strengths of our study were, i.e., the use of activities based on real patient data, the use of a phantom with a fixed configuration, the use of parts of standardized phantoms, the use of a clinically used gamma probe and optical navigation system, and incorporation of test sessions into the study. To the best of our knowledge, our study was the first who studied detectability of lymph nodes in a phantom using activities based on real patient data. The phantom used had a fixed configuration, which provided equality between the experiments and readers. Therefore, due to the combination of the patient based activities and the phantom used, we were able to test our hypothesis, without bias of prior knowledge. By using components of standardized phantom to create our phantom, we increased the reproducibility of our study. Since we used a clinically used gamma probe and optical navigation system, our results are relevant for clinical practice. In addition, we incorporated test sessions for the readers, therefore we eliminated the influence of learning effect from the experiments.

Our study also had some limitations. First, we used a simplified phantom to study the effect of distance and background activity on detectability of positive lymph nodes. A

simplified phantom does not mimic the situation in real life, especially because the phantom used was rigid, when in fact the situation in real life is non-rigid. The non-rigidity was compromised in the phantom study aimed at hybrid navigation by inducing a 9 mm shift in sphere location as compared to the prior performed scan. Second, we did not propose a fixed strategy to the readers on how to perform the navigation using the gamma probe. The absence of a fixed navigation strategy might have had an influence on the results. To study this influence, the phantom study could be performed again but now with a fixed strategy. Third, all readers had different backgrounds and none of them was a prostate surgery expert. The results could have varied when the experiments were performed by prostate surgery experts. To prove the results, the phantom study could be performed again by prostate surgery experts. fourth, the phantom experiment aimed at hybrid navigation has been performed singular. We have chosen to do this experiment singular since we expected that duplication of the experiment would lead to bias as a result of prior knowledge.

Our results indicate that hybrid navigation, using radio- and image-guidance, is a promising technique to distinguish affected from unaffected lymph nodes during PLND. As a result of specific targeting, less lymph nodes have to be dissected, which may reduce the number of complications and overtreatment. In our study we used navigation methods which are already used in clinical practice, therefore the translation to clinic of our approach will be relatively easy.

3.6. Conclusion

Both radio- and image-guidance are feasible techniques to distinguish affected form unaffected lymph nodes in the pelvic region during surgery. Radio-guidance becomes more accurate at a decreasing distance to the target. However, background activity has a significant influence on the accuracy. Image-guidance, on the other hand, provides real-time visual feedback allowing navigation to a target, but is sensitive to tissue shift. Hybrid navigation, in which radio- and image-guidance are combined, combines the advantages of both techniques and therefore seems to be feasible and superior compared to radio- and image-guidance alone.

4. Fluorescence detection

4.1. Introduction

As a result of our first three phantom experiments we see added value for the application of hybrid navigation for tPLND. In these first phantom experiments we focused on hybrid navigation in which radio- and image-guided navigation are combined. However, these two techniques could also be combined with fluorescence-guidance. Fluorescence-guidance is a technique in which a fluorescent dye emits in a certain part of the light spectrum. This specific signal can be detected with a fluorescence camera, after which the fluorescent signal can be displayed on a screen. This technique is particularly suitable for intra-operative delineation of tumor borders and could be used in combination with radioactivity. By labeling a fluorescent marker to a PSMA ligand, specific targeting of PCa lesions could be performed. In a preclinical study by Kovar et al. strong specific fluorescent signal was seen in PSMA positive tumors in mice after injection of a 800CW labeled PSMA ligand (YC-27 800CW) [70]. Wang et al. observed the same strong specific fluorescent signal using another PSMA ligand (PSMA-1) which they labeled with 800CW as well [71]. Besides single labeling, dual-labeled PSMA ligands are being studied. Baranski et al. studied ^{68}Ga-PSMA-11-IRDye800CW. This dual-labeled ligand showed a high uptake in PSMA specific tissue and had rapid background clearance [72]. Although these studies show the promising character of specific targeting using fluorescence, the penetration depth of the fluorescent marker has a significant impact on the detectability of lymph nodes during surgery.

In our third experiment we showed that, with a shift of 9 mm in real life compared to the pre surgery situation, a positive lymph node is identified incorrectly by almost 50% of the readers using image-guidance alone. In literature the penetration depth of near-infrared fluorescent dyes such as 800CW is estimated at a maximum of 10 mm [43]. However, in clinical practice a penetration depth of only 2 to 3 mm has been seen. Therefore, in order to test the applicability of fluorescence-guidance in combination with image- or radio-guidance, we need to study the penetration depth in tissue of 800CW.

In this experiment we studied the penetration depth of three different concentrations of 800CW in three types of tissue i.e.; muscle, fat and connective tissue.

4.2. Methods

To determine the penetration depth of 800CW in muscles, fat and connective tissue, an experimental setup was designed.

4.2.1. Fluorescent dye determination

For the determination of the fluorescent dye concentration, we used data found in literature. In literature a minimum PSMA receptors expression on tumor cell of 3700 is described [73], whereas a maximum of 1.7 million receptors was found [74]. Assuming a logarithmic distribution of the receptor expressing, we estimated an average expression of 300,000 PSMA receptor on tumor cells. Since in a tumor lesion of 1 cm^3 approximately 10^9

tumor cells are present [75], on average $3x10^{14}$ PSMA receptors are being expressed in a tumor lesion of 1 cm^3. Taking the Avogadro constant ($6.02214x10^{23}$) in mind, we found that a concentration of 0.5 µM 800CW is required to bind all receptors. Since 0.5 µM is an estimation of the clinically expected concentration and therefore other concentrations might be found in clinical practice as well, we studied a range of concentrations starting at 50 µM to 0.005 nM. The upper limit of 50 µM was chosen based on a study performed by van Willigen et al. [76].

4.2.2. Experimental design and data acquisition

24 Eppendorf tubes of 500 µL were in triplet filled with a 50 µM, 5 µM, 0.5 µM, 50 nM, 5 nM, 0.5 nM and 0.05 nM solution of 800CW (LI-COR, Leusden, The Netherlands) dissolved in Phosphate Buffered Saline (PBS). A circular matte phantom was used in which eight 500 µL Eppendorf tubes could be fixated (Figure 6). For each Eppendorf tube two holes with a radius of 5 and 3 mm were present at the surface of the phantom, through which the fluorescence signal could be observed (Figure 6). A fluorescence camera (Quest Spectrum, Quest Medical Imaging, Middenmeer, The Netherlands) was positioned at a height of 10 cm above the phantom. A slice of meat (muscle ±1 mm, connective tissue ±1.6 mm and fat ±1.6 mm) was placed on top of the phantom, hereafter an image capture was made with the camera (Fluorescence gain 25 dB, Fluorescence exposure 300 ms, Color gain 3.0 dB and Color exposure 6000 ms). After the first imaging session, another slice of meat was placed on top of the first slice of meat followed by a second imaging session. These steps were repeated until no fluorescent signal could be observed anymore (determined by one observer). The experiment was performed in triplet for all three different tissue types i.e., fat, muscle and connective tissue.

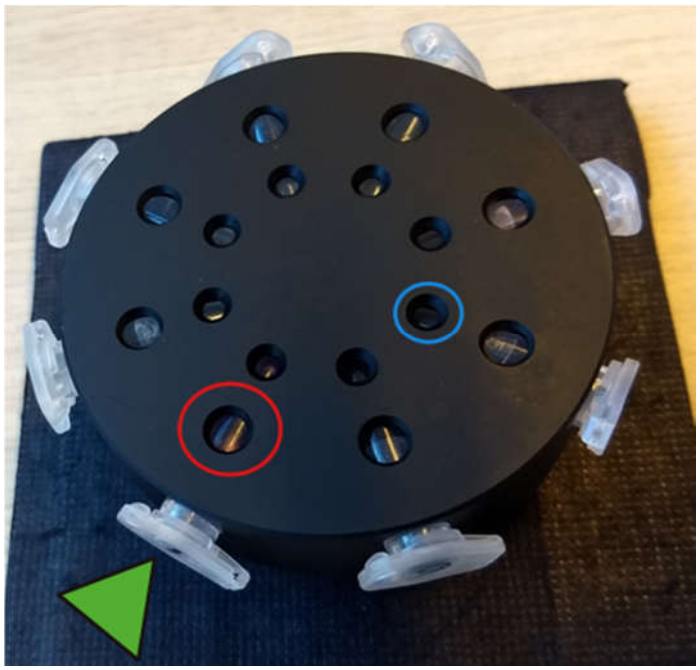

Figure 6: Image of the phantom in which eight Eppendorf tubes can be placed (green arrow). For each Eppendorf tube two holes with a radius of 5 (red circle) and 3 mm (blue circle) were present in the circular structure, through which the fluorescence signal could be observed.

4.2.3. Data analysis

To study and compare the intensity of the fluorescent signal at different tissue thicknesses, circular ROIs, with a radius of 50 pixels, were drawn in the circular holes with a radius of 5 mm in each frame. All frames had a size of 1080x720 pixels. In addition to the ROIs of the fluorescent signal, same sized ROIs were drawn in the middle of the phantom on every frame as well. These ROIs were drawn to indicate the mean pixel value of the background. A pixel value of 0 indicates black and a pixel value of 255 indicates white. To be able to compare the fluorescent signal between the different experiments, the mean pixel value of the background was subtracted from the mean pixel values of the fluorescence ROIs.

4.3. Results

At the starting point, where no slice of meat was placed on top of the phantom, a visible fluorescent signal could be observed for 50 µM, 5 µM, 0.5 µM and 50 nM (Figure 7). Since we were not able to visibly detect the signal of the other concentrations, we decided to limit our analysis to the four visibly detectable concentrations. The penetration depth in muscle tissue of the different concentrations which could be visibly detected are shown in Figure 7.

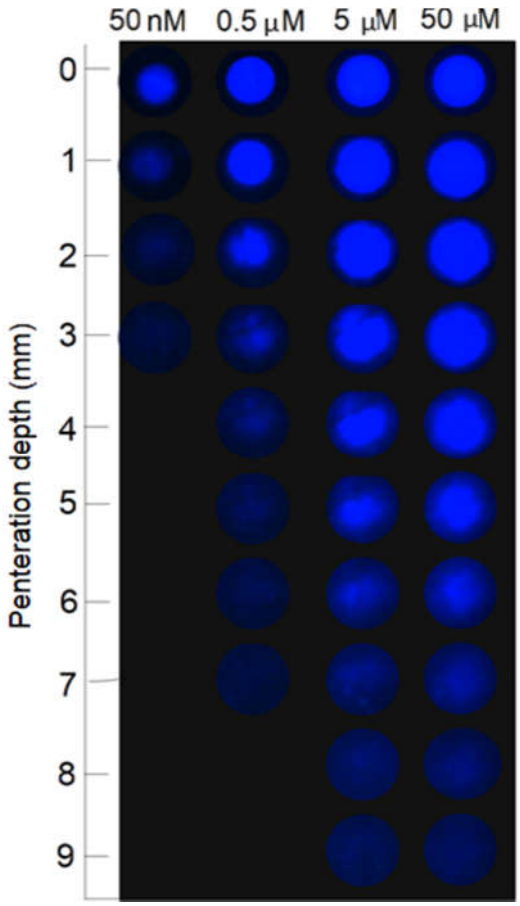

Figure 7: Penetration depth in muscle tissue for 50 µM, 5 µM, 0.5 µM and 50 nM IRDye 800CW dissolved in PBS measured at 10 cm camera distance, with a fluorescence gain of 25 dB, fluorescence exposure of 300 ms, color gain of 3.0 dB and color exposure of 6000 ms.

The detection limit was set at two times the mean pixel value of the background, based on visual detection of one observer. The detection limit was set on 20.

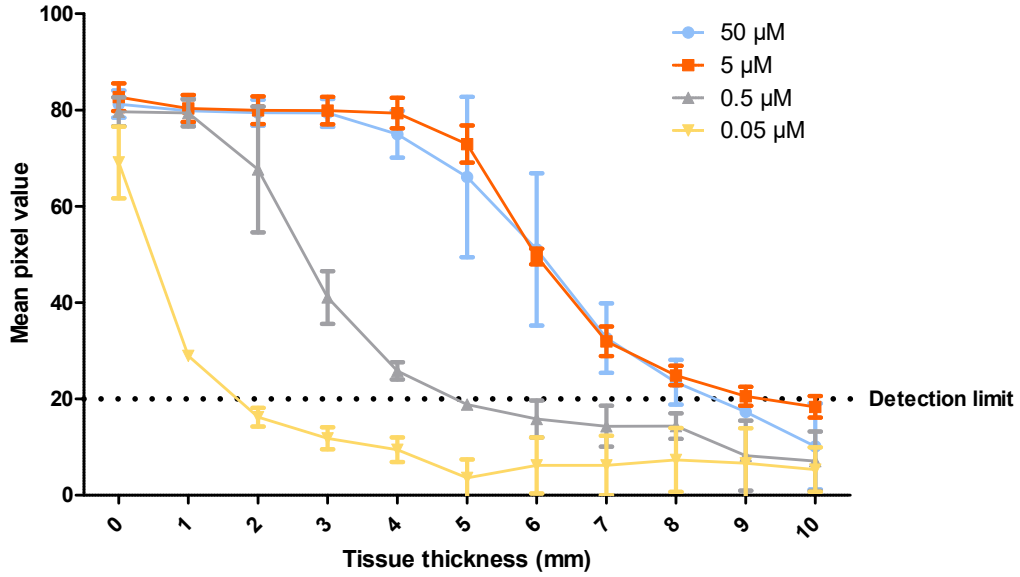

Figure 8: Penetration depth in muscle tissue for 50 µM, 5 µM, 0.5 µM and 50 nM IRDye 800CW dissolved in PBS, the degree of fluorescent signal is expressed in mean pixel value.

A tissue penetration depth of 8 mm was obtained in muscle tissue for both 50 and 5 µM (Figure 8). For 0.5 µM and 50 nM, penetration depths of respectively 4.8 mm and 1.6 mm were found in muscle tissue. For all concentrations we observed a smaller penetration depth in fatty and connective tissue compared to muscle tissue (Figure 9). Looking specifically at the clinical expected concentration of 0.5 µM, a penetration depth of 3 mm in connective tissue and of 2.3 mm in fatty tissue could be observed.

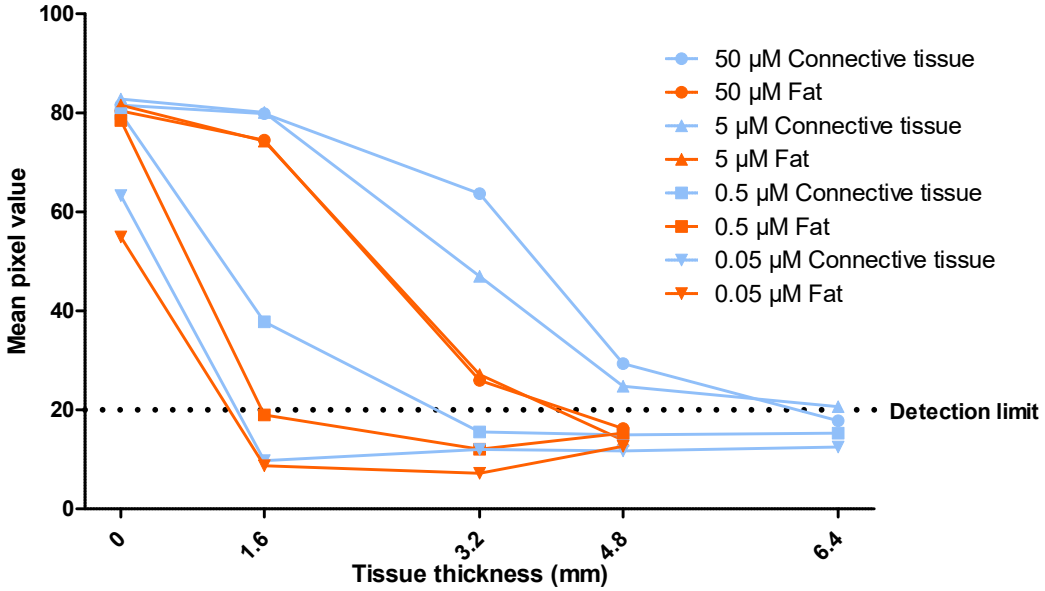

Figure 9: Penetration depth in connective tissue (blue) and fat (red) for 50 µM, 5 µM, 0.5 µM and 50 nM IRDye 800CW dissolved in PBS, the degree of fluorescent signal is expressed in mean pixel value.

4.4. Discussion

The results of our study show that a maximum penetration depth of 8 mm can be obtained for a 800CW concentration of 50 and 5 µM. This maximal penetration depth was seen in muscle tissue. For the clinically expected concentration of 0.5 µM a penetration depth of 2.3 to 4.8 mm could be obtained dependent on the tissue type.

Van Willigen et al. showed that with a concentration of 50 µM penetration depths of 6 to 9 mm can be achieved using near-infrared fluorescent dyes [76]. Our results show penetration depths of 4.5 mm in fatty tissue to 8 mm in muscles, and therefore are comparable to the results of van Willingen et al. However, since the maximum PSMA receptor expression is limited to 1.7 million receptors on one tumor cell [73], a maximum concentration of 28 µM could theoretically be achieved. Therefore, although in sentinel node procedures a concentration of 50 µM might be seen since these procedures are PSMA receptor independent, these concentrations will never be seen in a targeted approach.

Looking at Figure 8 and Figure 9, it can be observed that for all three tissue types a detection plateau is reached at a mean pixel value of around 80. Taking the mean pixel value course of the 0.5 µM and 50 nM lines into account, we might expect a higher maximal mean pixel value in the higher 800CW concentrations. However, since our analyses are based on pixel values, the actual fluorescence signal might be more prone, but since the maximal pixel value of the blue color has already been reached, this higher fluorescent signal could not be quantified using our method.

The strengths of our study were, i.e., the use of a clinical fluorescence camera, estimation of fluorescence concentrations based on PSMA receptor expression and comparison of clinically expected concentrations with concentrations tested in literature. To the best of our knowledge, our study was the first who studied the penetration depth of 800CW with fluorescence concentrations based on PSMA receptor expression. Besides concentrations based on PSMA receptor expression, we also used a clinically used fluorescence camera. By using this clinically used camera, we were able to study penetration depth as it would be in real patients. By comparing the penetration depth of our own estimated expected clinical concentration with a concentration used in literature, we were able to correlate our results with the results found in literature.

Our study also had some limitations. First, we used prepared meat products to study the penetration depth in fat, muscles and connective tissue. Although these slices of tissue do consist of the tissue types to be tested, they are processed and therefore do not entirely correspond to human tissue. This could have influenced our results. To overcome this limitation, unprocessed human tissue, which has to be sliced in thin slices, could be used. However, by the use of human tissue, more rules have to be met, providing a more complex study. Second, the thickness of the used meat slices differed between the different tissue types, introducing difficulties in comparing the result. This could be overcome by using the same slice thicknesses.

4.5. Conclusion

Our results indicate that 800CW can be used to localize tumor lesions in lymph nodes which are surrounded by a thin layer of tissue using a clinical fluorescence camera. Although a clinical fluorescence camera is already available, allowing a relatively easy translation into clinic, the dual-labeled 800CW-^{99m}Tc-PSMA tracer is not ready yet, at our institution.

5. Clinical application

For the clinical application of tPLND a clinical pilot study will be designed. This pilot study will focus on radio-guidance during ePLND using the small molecule MIP-1404 which will be labeled with ^{99m}Tc.

5.1. Clinical relevance

In clinical practice, ePLND is performed in all PCa patients with a risk of 5% or higher to develop lymph node metastases [17]. To perform an adequate and representative pathology sample on average 20 lymph nodes have to be dissected [19]. Although these numbers are met in clinical practice, lymph node metastases are still being missed, causing metastases within a couple of years. Surgeons face insufficient removal of the metastatic lymph nodes as a result of limited feedback during surgery. Pre-surgical imaging does not always reveal all metastatic lymph nodes and lesions seen on imaging cannot always be identified during surgery. Therefore, specific targeting of metastatic lymph nodes might be beneficial.

Specific targeting of PCa lesions using small-molecules with a high affinity of binding to PSMA could ensure a complete removal of metastatic lymph nodes. MIP-1404 is such a small-molecule which can be labeled with ^{99m}Tc. The pharmacokinetics and biodistribution of this small-molecule have already been studied in patients and show favorable results [65]. In this clinical pilot study we will study the feasibility, accuracy and safety of intra-operative gamma detection in ePLND patients.

5.2. Objectives

Primary objective: To assess the feasibility, accuracy and safety of intra-operative gamma detection in patients with prostate cancer and a more than 5% risk of metastases who will undergo ePLND.

Secondary objectives: To assess whether additional malignant lymph nodes can be identified using intra-operative gamma detection.

5.3. Patient population

5.3.1. Population

In this study, 20 patients with prostate cancer and a more than 5% risk of metastases scheduled for ePLND will be included. Patients will be recruited from the outpatient clinic of the Radboudumc. Yearly more than 100 ePLND procedures are performed at the Radboudumc. The expected inclusion rate is about 10 per year. Therefore, we expect that the study can be completed within two years.

5.3.2. Inclusion criteria

In order to be eligible to participate in this study, a subject must meet each of the following criteria:

- Age ≥ 18
- Male
- Prostate cancer
- Scheduled for ePLND

5.3.3. Exclusion criteria

A potential subject who meets any of the following criteria will be excluded from participation of the study:

- Non PSMA positive tumors
- Administration of a radionuclide within 10 physical half-lives prior to study enrollment

5.4. Clinical design

This is a single center, open label, single arm intervention study. In total, 20 patients with prostate cancer and a more than 5% risk of metastases scheduled for ePLND will be included.

Patients will receive a single intravenous dose of ^{99m}Tc-MIP-1404 approximately 20 hours prior to surgery [65]. 20 hours after injection, patients will undergo standard ePLND extended with the use of gamma detection. Gamma detection performed in vivo prior to resection and ex vivo on the resected tissue. All additional removal of tissue on the basis of gamma detection will be closely monitored and registered by a researcher.

After surgery, the samples of resected tissue will be analyzed by the pathology department.

6. General discussion

In clinical practice, patients with a chance of 5 percent or higher to develop metastases are subjected to ePLND [17]. Although ePLND shows positive results, lymph node metastases still remain in the pelvic and high complication rates are seen [16, 22]. The purpose of my thesis was to study a navigation technique to identify potential lymph node metastases in patients with prostate cancer during lymph node dissection, that can; perform specific targeting, capture soft tissue shift, provide real-time feedback and be accurate.

In **chapter 2** we performed a literature review on navigation methods used in clinical practice. First, we looked at sentinel node procedures. Although this technique is relatively easy, the disadvantages of a sentinel node procedure, e.g. the nonspecific character and blockage of accumulations due to metastasis, outweigh its advantages. Making this technique not the technique of choice to navigate to pelvic lymph nodes. In addition to the sentinel node procedure we have found three navigation methods which have potential, i.e., specific targeting using PSMA ligands, labeled with radioactivity and/or a fluorescent dye and image-guided navigation. The advantage of the use of PSMA ligands is the specific targeting, to lesions overexpressing PSMA. Radio and fluorescence labeling have potential, both with their own advantages. The biggest advantage of radio labeled PSMA is its wide detection range. However, since the detection is based on an acoustic signal it can be hard to discriminate the exact location. Fluorescence, on the other hand, is based on visual detection, whereby the detection is very precise. However, the disadvantage of fluorescence is its low penetration depth of only a couple of millimeters. Therefore, in our opinion, a combination of both techniques would be beneficial.

The third potential technique is image-guided navigation. Image-guided navigation is especially used in rigid tissue, e.g. bones, but also has applications in soft tissue[29]. Image-guidance is a potential navigation technique, since suspicious lesions can be annotated prior to surgery allowing targeted surgery. Another advantage of image-guidance is the real-time feedback during surgery. The disadvantages of image-guided navigation in non-rigid tissue is the non-continuous registration of tissue shift, which might lead to incorrect navigation. We suggest that a combination of these techniques will result in specific targeting, capturing of soft tissue shift, real-time feedback and accuracy.

In **chapter 3** we performed a phantom study aimed at hybrid navigation. The study was divided in a radio-guidance part and an image-guidance part. In the radio-guidance part we observed a significant influence of background activity on the detectability of both the spheres with and without a radioactive solution. This is in accordance with studies in which the negative influence of background activity has been observed in sentinel node procedures [44]. It also turned out that the distance of probe placement relative to the spheres had a significant influence on detectability. The correct identification of spheres increased as the probe could be placed closer to the spheres. This effect was seen in both the experiments with

and without background activity. Therefore, both distance and background activity are of influence on detectability and mutual reinforcement has been seen in the experiment with background activity.

In the image-guidance part we applied a shift of 9 mm compared to the original situation. Our results indicate that in almost 50% of the cases positive lymph nodes will be identified incorrect if image-guided navigation is applied alone. In other words in approximately 50% of the cases a wrong lymph node would probably be removed in case only the annotated lymph nodes would be removed. When radio- and image-guidance are combined we see an enormous increase in correct identifications, even up to a 100% correctly identification. Although our results are based on a static set up, these results indicate the added value of hybrid navigation in which radio- and image-guidance are applied.

In **chapter 4** we studied the penetration depth of different concentrations 800CW in three types of tissue i.e., connective tissue, fat and muscles. Using data found in literature, a clinical expected concentration of 0.5 µM 800CW could be calculated. Our results showed a larger penetration depth in muscles compared to fat and connective tissue. Looking specifically at the clinical expected concentration, we observed penetration depths of 2 to 5 mm. These results indicate that fluorescence-guidance is feasible to detect lymph node metastases.

In **chapter 5** an overview of a clinical trial was drawn. This trail is aimed at targeted radio-guided navigation, and will be performed as a feasibility study for the use of a dual-labeled PSMA ligand.

The research in this thesis provides insight on different navigation methods applicable for PLND. Our results show the potential added value of the different navigation methods. Combining the three techniques might provide specific, precise and accurate navigation. However, the best combination of techniques will depend on the clinical objective of the surgeon. In case the surgeon wants to identify all metastatic lesions regardless of these lesions were already found with imaging, radio-guidance will add the largest value. On the other hand in case the clinical objective is localization of already identified metastatic lesions, the largest added value might be seen in fluoresce- and image-guidance.

6.1. Future perspectives

Hybrid navigation for PLND is still in development. In this thesis we showed the potential value of radio-, fluorescence- and image-guidance and their combinations. Clinical trials have to be performed to further evaluate the clinical impact of hybrid navigation for PLND.

In the first clinical trial the commercially available ligand MIP-1404 will be used. This ligand can only be labeled with a radiotracer (^{99m}Tc), whereby hybrid navigation, in which radio- and fluorescence-guidance are used, cannot be studied. Preclinical studies are already performed according to dual-labeled PSMA ligands [72] and anti-bodies [77, 78]. These studies demonstrate the potential value of the combination of fluorescence- and radio-guidance. Further research is needed to correlate hybrid navigation to histology and to prepare PSMA ligands for in human application. At this moment PSMA ligands suitable for dual-labeling are under construction at our department. When the dual-labeled ligands are applicable for in human use, a clinical trial has to be composed to further evaluate the additional value of this hybrid approach for overall survival.

The moment of injection of labeled PSMA ligands is of great importance to obtain good clinical outcomes. Since we demonstrated influence of background activity on de detectibility of positive lymph nodes, tumor to background ratios have to be high to limit interference of background activity with positive lymph nodes. In the first clinical trial the PSMA ligand MIP-1404 will be used. The favorable time point of injection of MIP-1404 has been studied once. This study demonstrated favorable characteristics at a time point of around 20 hours prior to surgery [65]. To confirm these findings the biodistribution and injection point has to be studied in more detail during the first clinical trial. For a second clinical trial it is intended to use the dual-labeled PSMA ligand which is under construction at this moment. Therefore, since the biodistribution is ligand specific, the favorable injection time point of the dual-labeled PSMA ligand has to be studied as well during the second clinical trial.

In this thesis we demonstrated the potential value of the use of image-guided navigation in combination with radio-guidance. Limited research has been performed regarding this type of hybrid navigation for PLND. Research that has been performed is mainly focused on hybrid navigation using image-guidance in combination with nanocolloid instead of targeted radio-guidance [44, 69]. Additional image-guidance might increase the time of the procedure at first, but when it becomes more routinely this increase in time will probably decrease. On the other hand, the efficiency and effectiveness might increase using this hybrid approach. Further research has to be performed to prove the added value of targeted hybrid navigation. Therefore, clinical trials have to be composed for hybrid navigation using image-guidance with a ^{99m}Tc labeled PSMA ligand and with a dual-labeled PSMA ligand.

In further clinical studies it is important to evaluate the workflow of image-guidance. The work environment at the operation theatre might be made easier by implementation of augmented reality. Augmented reality is a technique which has already been incorporated in image-guidance, but is still in its development. Augmented reality allows the surgeon to visualize the surgery field on the patient without looking at a screen.

In the experiment aimed at penetration depth of 800CW we used a clinically available fluorescence camera which can be used for open procedures, but which is not suitable for laparoscopic procedures. We know that laparoscopic fluorescence cameras are able to detect less fluorescent signal compared to the fluorescence camera used in the open setting. However, to quantify the smaller penetration depth using a laparoscopic fluorescence camera instead of an open fluorescence camera, the experiment has to be repeated using a laparoscopic fluorescence camera.

Improvements may also be made in annotating histological tissue samples. Nowadays histological tissue samples are pinned to a tissue board which is based on the standard anatomy of the nodal zones. However, since the anatomy varies between patients, the layout of the tissue board should be patient specific. Such a patient specific tissue board can be obtained by using pre-operative imaging as a map and translate it to a tissue board.

References

1. Ferlay, J., et al., *Cancer incidence and mortality worldwide: sources, methods and major patterns in GLOBOCAN 2012.* Int J Cancer, 2015. **136**(5): p. E359-86.
2. Attard, G., et al., *Prostate cancer.* The Lancet, 2016. **387**(10013): p. 70-82.
3. Vidal-Sicart, S. and R.A. Valdes Olmos, *Sentinel node approach in prostate cancer.* Rev Esp Med Nucl Imagen Mol, 2015. **34**(6): p. 358-71.
4. Turkbey, B., et al., *Multiparametric prostate magnetic resonance imaging in the evaluation of prostate cancer.* CA Cancer J Clin, 2016. **66**(4): p. 326-36.
5. Zhang, S., et al., *2D Ultrasound and 3D MR Image Registration of the Prostate for Brachytherapy Surgical Navigation.* Medicine (Baltimore), 2015. **94**(40): p. e1643.
6. Budäus, L., et al., *Initial experience of 68 Ga-PSMA PET/CT imaging in high-risk prostate cancer patients prior to radical prostatectomy.* European urology, 2016. **69**(3): p. 393-396.
7. Widmark, A., et al., *Endocrine treatment, with or without radiotherapy, in locally advanced prostate cancer (SPCG-7/SFUO-3): an open randomised phase III trial.* The Lancet, 2009. **373**(9660): p. 301-308.
8. Wilt, T.J., et al., *The Prostate cancer Intervention Versus Observation Trial: VA/NCI/AHRQ Cooperative Studies Program# 407 (PIVOT): design and baseline results of a randomized controlled trial comparing radical prostatectomy to watchful waiting for men with clinically localized prostate cancer.* Contemporary clinical trials, 2009. **30**(1): p. 81-87.
9. Cary, K.C., et al., *Nationally representative trends and geographic variation in treatment of localized prostate cancer: the Urologic Diseases in America project.* Prostate Cancer Prostatic Dis, 2015. **18**(2): p. 149-54.
10. Joung, J.Y., I.C. Cho, and K.H. Lee, *Role of pelvic lymph node dissection in prostate cancer treatment.* Korean J Urol, 2011. **52**(7): p. 437-45.
11. Siegel, R.L., K.D. Miller, and A. Jemal, *Cancer statistics, 2018.* CA Cancer J Clin, 2018. **68**(1): p. 7-30.
12. Briganti, A., et al., *Lymphatic spread of nodal metastases in high-risk prostate cancer: The ascending pathway from the pelvis to the retroperitoneum.* Prostate, 2012. **72**(2): p. 186-92.
13. Godoy, G., et al., *Pelvic lymph node dissection for prostate cancer: frequency and distribution of nodal metastases in a contemporary radical prostatectomy series.* J Urol, 2012. **187**(6): p. 2082-6.
14. Fossati, N., et al., *The Benefits and Harms of Different Extents of Lymph Node Dissection During Radical Prostatectomy for Prostate Cancer: A Systematic Review.* Eur Urol, 2017. **72**(1): p. 84-109.
15. Bader, P., et al., *Disease progression and survival of patients with positive lymph nodes after radical prostatectomy. Is there a chance of cure?* The Journal of urology, 2003. **169**(3): p. 849-854.
16. Mattei, A., et al., *The template of the primary lymphatic landing sites of the prostate should be revisited: results of a multimodality mapping study.* European Urology, 2008. **53**(1): p. 118-125.

17. Heidenreich, A., et al., *EAU guidelines on prostate cancer. Part 1: screening, diagnosis, and local treatment with curative intent—update 2013.* European urology, 2014. **65**(1): p. 124-137.
18. Briganti, A., et al., *Pelvic lymph node dissection in prostate cancer.* European urology, 2009. **55**(6): p. 1251-1265.
19. Weingartner, K., et al., *Anatomical basis for pelvic lymphadenectomy in prostate cancer: results of an autopsy study and implications for the clinic.* J Urol, 1996. **156**(6): p. 1969-71.
20. Bader, P., et al., *Is a limited lymph node dissection an adequate staging procedure for prostate cancer?* The Journal of urology, 2002. **168**(2): p. 514-518.
21. Heidenreich, A., Z. Varga, and R. Von Knobloch, *Extended pelvic lymphadenectomy in patients undergoing radical prostatectomy: high incidence of lymph node metastasis.* J Urol, 2002. **167**(4): p. 1681-6.
22. Briganti, A., et al., *Complications and other surgical outcomes associated with extended pelvic lymphadenectomy in men with localized prostate cancer.* Eur Urol, 2006. **50**(5): p. 1006-13.
23. Brenot-Rossi, I., et al., *Radioguided sentinel lymph node dissection in patients with localised prostate carcinoma: influence of the dose of radiolabelled colloid to avoid failure of the procedure.* Eur J Nucl Med Mol Imaging, 2008. **35**(1): p. 32-8.
24. Meinhardt, W., et al., *Laparoscopic sentinel node dissection for prostate carcinoma: technical and anatomical observations.* BJU Int, 2008. **102**(6): p. 714-7.
25. Weckermann, D., et al., *Limitations of radioguided surgery in high-risk prostate cancer.* Eur Urol, 2007. **51**(6): p. 1549-56; discussion 1556-8.
26. Robu, S., et al., *Preclinical Evaluation and First Patient Application of 99mTc-PSMA-I&S for SPECT Imaging and Radioguided Surgery in Prostate Cancer.* J Nucl Med, 2017. **58**(2): p. 235-242.
27. Schottelius, M., et al., *[(111)In]PSMA-I&T: expanding the spectrum of PSMA-I&T applications towards SPECT and radioguided surgery.* EJNMMI Res, 2015. **5**(1): p. 68.
28. Brouwer, O.R., et al., *Image navigation as a means to expand the boundaries of fluorescence-guided surgery.* Physics in Medicine and Biology, 2012. **57**(10): p. 3123-3136.
29. Rassweiler, J., et al., *Surgical navigation in urology: European perspective.* Curr Opin Urol, 2014. **24**(1): p. 81-97.
30. Wit, E.M.K., et al., *Sentinel Node Procedure in Prostate Cancer: A Systematic Review to Assess Diagnostic Accuracy.* Eur Urol, 2017. **71**(4): p. 596-605.
31. Mannweiler, S., et al., *Heterogeneity of prostate-specific membrane antigen (PSMA) expression in prostate carcinoma with distant metastasis.* Pathol Oncol Res, 2009. **15**(2): p. 167-72.
32. Wright, G.L., Jr., et al., *Upregulation of prostate-specific membrane antigen after androgen-deprivation therapy.* Urology, 1996. **48**(2): p. 326-34.
33. Perner, S., et al., *Prostate-specific membrane antigen expression as a predictor of prostate cancer progression.* Human Pathology, 2007. **38**(5): p. 696-701.
34. Rauscher, I., et al., *„PSMA-radioguided surgery "beim lokal begrenzten Prostatakarzinomrezidiv.* Der Urologe, 2017. **56**(1): p. 18-23.
35. Schaal, K., et al., *Performance of 111In-PSMA-ligand radioguided surgery for identification of lymph node metastases: Correlation of tracer uptake and*

histopathology based on 310 single lymph nodes separated from lymphadenectomies in prostate cancer patients. European Urology Supplements, 2017. **16**(3): p. e1515-e1516.
36. van den Berg, N.S., et al., *Multispectral Fluorescence Imaging During Robot-assisted Laparoscopic Sentinel Node Biopsy: A First Step Towards a Fluorescence-based Anatomic Roadmap.* Eur Urol, 2017. **72**(1): p. 110-117.
37. KleinJan, G.H., et al., *Optimisation of fluorescence guidance during robot-assisted laparoscopic sentinel node biopsy for prostate cancer.* Eur Urol, 2014. **66**(6): p. 991-8.
38. Marshall, M.V., et al., *Single-dose intravenous toxicity study of IRDye 800CW in Sprague-Dawley rats.* Mol Imaging Biol, 2010. **12**(6): p. 583-94.
39. Harada, N., et al., *Preparation of Asymmetric Urea Derivatives that Target Prostate-Specific Membrane Antigen for SPECT Imaging.* Journal of Medicinal Chemistry, 2013. **56**(20): p. 7890-7901.
40. Matsuoka, D., et al., *Structure–activity relationships of succinimidyl-Cys-C (O)-Glu derivatives with different near-infrared fluorophores as optical imaging probes for prostate-specific membrane antigen.* Bioorganic & Medicinal Chemistry, 2018.
41. Matsuoka, D., et al., *Synthesis and evaluation of a novel near-infrared fluorescent probe based on succinimidyl-Cys-C(O)-Glu that targets prostate-specific membrane antigen for optical imaging.* Bioorganic & Medicinal Chemistry Letters, 2017. **27**(21): p. 4876-4880.
42. Barrese, J.C. and J.M. Henderson, *The neurosurgical origins of image-guided surgery.* Current Problems in Surgery, 2015. **52**(12): p. 476-520.
43. Kim, S., et al., *Near-infrared fluorescent type II quantum dots for sentinel lymph node mapping.* Nature biotechnology, 2004. **22**(1): p. 93.
44. van den Berg, N.S., et al., *Sentinel lymph node biopsy for prostate cancer: a hybrid approach.* J Nucl Med, 2013. **54**(4): p. 493-6.
45. Wang, J., et al., *Augmented reality navigation with automatic marker-free image registration using 3-D image overlay for dental surgery.* IEEE transactions on biomedical engineering, 2014. **61**(4): p. 1295-1304.
46. Simpson, A.L., et al., *Comparison study of intraoperative surface acquisition methods for surgical navigation.* IEEE Trans Biomed Eng, 2013. **60**(4): p. 1090-9.
47. Ukimura, O., C. Magi-Galluzzi, and I.S. Gill, *Real-time transrectal ultrasound guidance during laparoscopic radical prostatectomy: impact on surgical margins.* The Journal of urology, 2006. **175**(4): p. 1304-1310.
48. Simpfendörfer, T., et al., *Augmented reality visualization during laparoscopic radical prostatectomy.* Journal of endourology, 2011. **25**(12): p. 1841-1845.
49. Mason, A., et al., *The accuracy of pedicle screw placement using intraoperative image guidance systems: A systematic review.* Journal of Neurosurgery: Spine, 2014. **20**(2): p. 196-203.
50. Billings, S., et al., *Minimally invasive registration for computer-assisted orthopedic surgery: combining tracked ultrasound and bone surface points via the P-IMLOP algorithm.* International journal of computer assisted radiology and surgery, 2015. **10**(6): p. 761-771.
51. Bernardeschi, D., et al., *Use of bone anchoring device in electromagnetic computer-assisted navigation in lateral skull base surgery.* Acta oto-laryngologica, 2013. **133**(10): p. 1047-1052.
52. Dello, S.A., et al., *Prospective volumetric assessment of the liver on a personal computer by nonradiologists prior to partial hepatectomy.* World J Surg, 2011. **35**(2): p. 386-92.

53. Cash, D.M., et al., *Incorporation of a laser range scanner into image-guided liver surgery: Surface acquisition, registration, and tracking.* Medical Physics, 2003. **30**(7): p. 1671-1682.
54. Zinser, M., et al. *Comparison of different registration methods for navigation in craniomaxillofacial surgery.* in *Perspective in Image-Guided Surgery* 2004.
55. Schlaier, J., J. Warnat, and A. Brawanski, *Registration accuracy and practicability of laser-directed surface matching.* Computer Aided Surgery, 2002. **7**(5): p. 284-290.
56. Peters, T. and K. Cleary, *Image-guided interventions: technology and applications.* 2008: Springer Science & Business Media.
57. Nijkamp, J., et al. *Image-guided navigation surgery for pelvic malignancies using electromagnetic tracking.* in *Medical Imaging 2016: Image-Guided Procedures, Robotic Interventions, and Modeling.* 2016. International Society for Optics and Photonics.
58. *Northern Digital Inc, Aurora Features.* 2018 13-02-2018]; Available from: https://www.ndigital.com/medical/products/aurora/#aurora-brochure.
59. Volonte, F., et al., *Console-integrated stereoscopic OsiriX 3D volume-rendered images for da Vinci colorectal robotic surgery.* Surg Innov, 2013. **20**(2): p. 158-63.
60. Nicolau, S., et al., *Augmented reality in laparoscopic surgical oncology.* Surg Oncol, 2011. **20**(3): p. 189-201.
61. Soler, L., et al., *Real-time 3D image reconstruction guidance in liver resection surgery.* Hepatobiliary Surg Nutr, 2014. **3**(2): p. 73-81.
62. Baumhauer, M., et al., *Navigation in endoscopic soft tissue surgery: perspectives and limitations.* J Endourol, 2008. **22**(4): p. 751-66.
63. Maurer, T., et al., *99m Technetium-based Prostate-specific Membrane Antigen–radioguided Surgery in Recurrent Prostate Cancer.* European Urology, 2018.
64. Lawal, I.O., et al., *Diagnostic sensitivity of Tc-99m HYNIC PSMA SPECT/CT in prostate carcinoma: A comparative analysis with Ga-68 PSMA PET/CT.* Prostate, 2017. **77**(11): p. 1205-1212.
65. Vallabhajosula, S., et al., *99mTc-labeled small-molecule inhibitors of prostate-specific membrane antigen: pharmacokinetics and biodistribution studies in healthy subjects and patients with metastatic prostate cancer.* J Nucl Med, 2014. **55**(11): p. 1791-8.
66. Nakamoto, M., et al., *Recovery of respiratory motion and deformation of the liver using laparoscopic freehand 3D ultrasound system.* Medical Image Analysis, 2007. **11**(5): p. 429-442.
67. Feuerstein, M., et al., *Intraoperative laparoscope augmentation for port placement and resection planning in minimally invasive liver resection.* IEEE Trans Med Imaging, 2008. **27**(3): p. 355-69.
68. Baumhauer, M., et al. *Soft tissue navigation for laparoscopic prostatectomy: Evaluation of camera pose estimation for enhanced visualization.* in *Medical Imaging 2007: Visualization and Image-Guided Procedures.* 2007. International Society for Optics and Photonics.
69. Bowles, H., et al., *Radioguided surgery and the GOSTT concept: From pre-operative image and intraoperative navigation to image-assisted excision.* Rev Esp Med Nucl Imagen Mol, 2017. **36**(3): p. 175-184.
70. Kovar, J.L., et al., *Pharmacokinetic and Biodistribution Assessment of a Near Infrared-Labeled PSMA-Specific Small Molecule in Tumor-Bearing Mice.* Prostate Cancer, 2014. **2014**: p. 10.

71. Wang, X., et al., *Development of targeted near-infrared imaging agents for prostate cancer.* Mol Cancer Ther, 2014. **13**(11): p. 2595-606.
72. Baranski, A.C., et al., *PSMA-11-Derived Dual-Labeled PSMA Inhibitors for Preoperative PET Imaging and Precise Fluorescence-Guided Surgery of Prostate Cancer.* J Nucl Med, 2018. **59**(4): p. 639-645.
73. Hernandez-Hoyos, G., et al., *MOR209/ES414, a Novel Bispecific Antibody Targeting PSMA for the Treatment of Metastatic Castration-Resistant Prostate Cancer.* Mol Cancer Ther, 2016. **15**(9): p. 2155-65.
74. Taylor, R.M., et al., *Prostate cancer targeting motifs: Expression of αvβ3, neurotensin receptor 1, prostate specific membrane antigen, and prostate stem cell antigen in human prostate cancer cell lines and xenografts.* The Prostate, 2012. **72**(5): p. 523-532.
75. Del Monte, U., *Does the cell number 109 still really fit one gram of tumor tissue?* Cell Cycle, 2009. **8**(3): p. 505-506.
76. van Willigen, D.M., et al., *Multispectral fluorescence guided surgery; a feasibility study in a phantom using a clinical-grade laparoscopic camera system.* Am J Nucl Med Mol Imaging, 2017. **7**(3): p. 138-147.
77. Lutje, S., et al., *Dual-Modality Image-Guided Surgery of Prostate Cancer with a Radiolabeled Fluorescent Anti-PSMA Monoclonal Antibody.* J Nucl Med, 2014. **55**(6): p. 995-1001.
78. Lutje, S., et al., *Development and characterization of a triple-modality anti-PSMA targeting agent for immuno-SPECT/CT, near-infrared fluorescence imaging and targeted photodynamic therapy of PSMA-expressing tumors.* Journal of Nuclear Medicine, 2016. **57**(supplement 2): p. 1203-1203.

Appendices

I. Additional analyses

Correctly identified positive spheres

For the first two experiments we also looked at the identification of the positive spheres only. So, what are the percentages of correctly identification of spheres if only the positive spheres are taken into account.

In the experiments with background activity there is a significantly larger percentage of uncertain identified spheres at a distance of 10 (18.93% ±18.73 vs 3.21% ± 8.23; p=0.001) and 5 cm (55.00% ± 29.61 vs 21.79% ± 22.15; p=0.01) compared to the experiments without background activity. At a distance of 10 cm to the spheres there is a significant larger percentage correctly identified spheres in the experiments with background activity compared to the experiments without background activity (85.71% ±27.66 vs 27.86% ±31.61; p=0.001). It should be taken into account that of the 85.71% correctly identified 68.93% was uncertain compared to an uncertainty of 17.86% of the 27.86% in the experiments without background activity.

In the experiments without background activity, a significant larger percentage correctly identified spheres can be identified at a distance of 5 compared to 10 cm (58.58% ±32.96 vs 27.86% ±31.61; p=0.05), at 0 compared to 10 cm (89.64% ±10.83 vs 27.86% ±31.61; p=0.001), and at 0 compared to 5 cm (89.64% ±10.83 vs 58.58% ±32.96; p=0.05). A significant larger percentage of active spheres were correctly identified as reasonably sure at a distance of 5 compared to 10 cm (38.57% ±29.18 vs 11.79% ±20.15; p=0.01), at 0 compared to 10 cm (86.43% ±13.22 vs 11.79% ±20.15; p=0.001), and at 0 compared to 5 cm (86.43% ±13.22 vs 38.57% ±29.18; p=0.001).

In the experiments with background activity, a significant larger percentage of spheres identified as reasonably sure can be observed at a distance of 0 compared to 10 cm (65.36% ±21.88 vs 16.78% ±29.33; p=0.001), and at 0 compared to 5 cm (65.36% ±21.88 vs 21.43% ±29.12; p=0.001). A significant lower percentage of uncertain identified spheres can be observed at a distance of 0 compared to 10 cm (18.93% ±18.73 vs 68.93% ±34.20; p=0.001) and at 0 compared to 5 cm (18.93% ±18.73 vs 55.00% ±29.61; p=0.01).

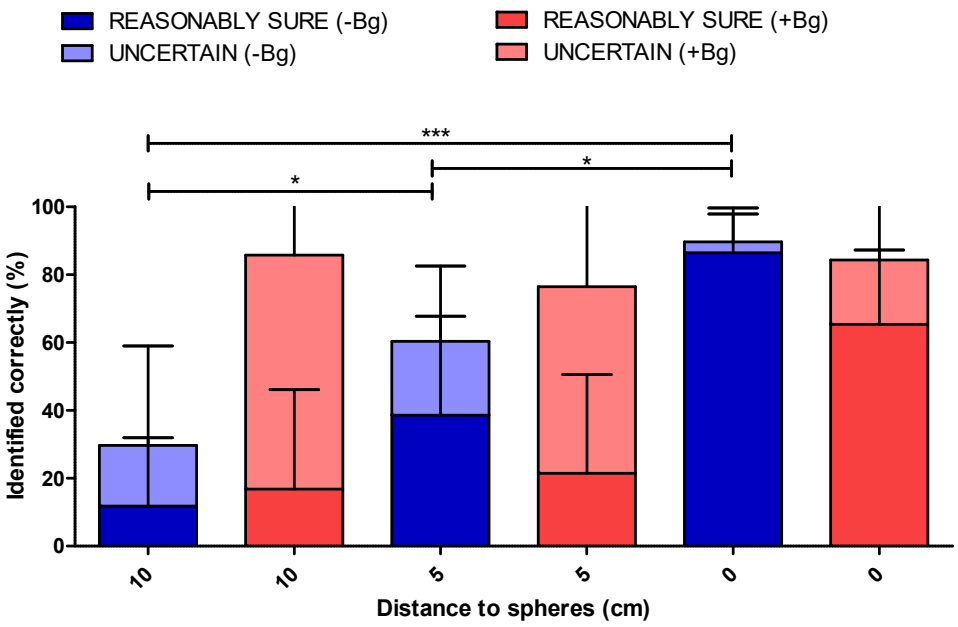

Figure 10: Percentages of correctly identified positive spheres for the experiments with (+Bg) and without background activity (-Bg) at three distances (10, 5 and 0 cm). Each bar is divided in; reasonably sure about their identification, and uncertain about their identification.

II. Image-Guided Navigation

The first step in optical navigation is making pre-operative imaging. In the context of our study we use PET/CT as pre-operative imaging. The PET/CT scan is used to annotate the positive lymph nodes and other relevant structures. In the operation theatre fudicial markers are used for location and orientation determination of the patient, scanner and surgical instruments. The fiducial markers used for infrared light navigation have at least three infrared reflecting spheres. The spheres of the fiducial markers reflect all of the infrared light that falls on the markers and are therefore seen by the camera of the optical navigation system (ONS) as white dots. Due to the fixed and unique configurations of the spheres on the different fiducial markers, the system recognizes the configurations as individual fiducial markers. Each object (patient (or phantom), scanner, surgical instruments) has its own coordinate system. These can be expressed relative to each other or to a world coordinate system through a relative 3D position and orientation. Our Coordinate systems are the gamma probe reference target (GRT), patient (or phantom) reference target (PRT) and Zeego reference target (ZRT) are of importance. The 3D positions and orientations can be expressed as 6D vectors. These 6D vectors are often referred to as 3D poses. These poses can be rewritten as 3D rigid transformations 4 x 4 matrices from the coordinate system of the ONS to the coordinate system of the respective targets (${}^{\mathrm{GRT}}T_{\mathrm{ONS}}$, ${}^{\mathrm{PRT}}T_{\mathrm{ONS}}$ and ${}^{\mathrm{ZRT}}T_{\mathrm{ONS}}$ respectively).

Registration has to be performed to link the pre-operative imaging data to the coordinate system of the ONS. This registration could be performed in two ways; either by using just the pre-operative imaging or by making a cone beam CT during surgery. In case only the pre-operative images are used, registration has to be performed by point paired and surface maTch. In this way the transformation matrix of the 3D position of the low dose CT of the PET/CT scan and the patient reference target can be written as:

$$ {}^{\mathrm{PRT}}T_{\mathrm{LDCT}} = {}^{\mathrm{PRT}}T_{\mathrm{ONS}} \left({}^{\mathrm{LDCT}}T_{\mathrm{ONS}}\right)^{-1} $$

In case a cone beam CT is made during surgery, the registration becomes slightly different. The Zeego cone beam CT is calibrated in such a way that according to the cone beam CT the transformation matrix between ZRT and the cone beam CT is known (${}^{\mathrm{ZRT}}T_{\mathrm{CBCT}}$). According to this calibration, the system knows the transformation between the ZRT and the ONS (${}^{\mathrm{ONS}}T_{\mathrm{ZRT}}$). Thereafter, the system uses the transformation between the Zeego and the ONS to obtain the transformation between the patient (or phantom) and the ONS (${}^{\mathrm{PRT}}T_{\mathrm{ONS}}$). Now the transformation matrix between the patient and the cone beam CT can be obtained by:

$$ {}^{\mathrm{ONS}}T_{\mathrm{CBCT}} = {}^{\mathrm{ONS}}T_{\mathrm{ZRT}}\, {}^{\mathrm{ZRT}}T_{\mathrm{CBCT}} $$

$$ {}^{\mathrm{PRT}}T_{\mathrm{CBCT}} = {}^{\mathrm{ONS}}T_{\mathrm{CBCT}}\, {}^{\mathrm{PRT}}T_{\mathrm{ONS}} $$

To know the position of the tip of the gamma probe a calibration step has to be performed. The calibration construct has three reflecting spheres with a unique geometry, therefore the

optical navigation system recognizes the calibration construct. The configuration and the diameter of the tip can be adjusted using the calibration construct. The calibration step will not correct for the 30° angle between the handle and the tip of the gamma probe. As a result of the calibration the transformation matrix from the tip of the gamma probe and the reference target of the gamma probe is created (${}^{\mathrm{TP}}T_{\mathrm{GRT}}$). Now the transformation between the tip of the gamma probe and the patient (or phantom) reference target can be obtained by:

$$ {}^{\mathrm{TP}}T_{\mathrm{PRT}} = {}^{\mathrm{TP}}T_{\mathrm{GRT}}\ {}^{\mathrm{GRT}}T_{\mathrm{PRT}} $$

Since the transformation between the patient and the CT scan (Cone beam CT or low dose CT) is already known, the transformation matrix between the tip of the gamma probe and the CT can be obtained by:

$$ {}^{\mathrm{TP}}T_{CT} = {}^{\mathrm{TP}}T_{\mathrm{PRT}}\ {}^{\mathrm{PRT}}T_{CT} $$

A schematic overview of these transformation steps can be found in Figure 12. Figure 11 displays the individual components of the experimental setup of the hybrid navigation phantom study.

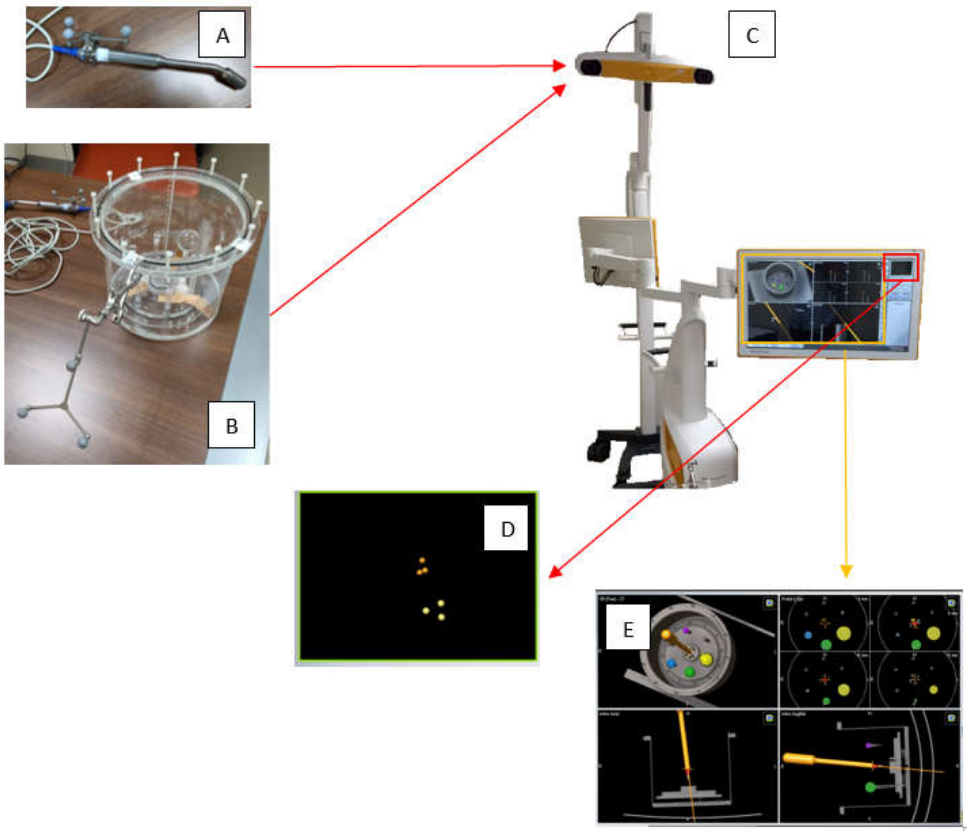

Figure 11: Individual components of the experimental setup of the phantom study. A) Gamma probe with fiducial marker, B) phantom with fiducial marker, C) Brainlab navigation system, D) display of reflecting spheres on screen, and E) Display of navigated gamma probe on screen.

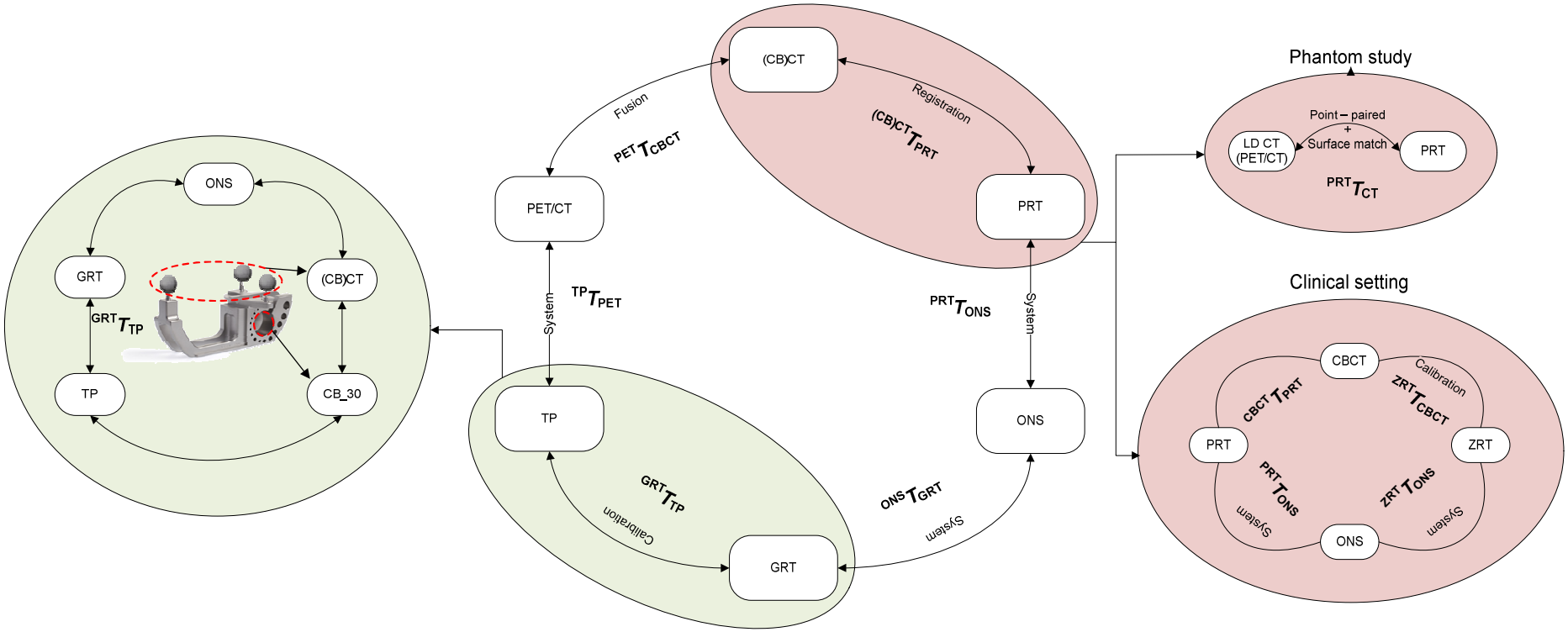

Figure 12: Schematic overview of the transformations matrices of the optical navigation system. In pink the registration steps split up into a registration part of the phantom study and for a clinical application. In green the calibration step of the gamma probe, the calibration is performed by the construct displayed in the green circle. CBCT = Cone Beam CT, PRT = Patient (or Phantom) Reference Target, ONS = Optical Navigation System, GRT = Gamma probe Reference Target, TP = Tip gamma Probe, LD CT = Low Dose CT and ZRT = Zeego Reference Target